UNIVERSITÀ
DI PAVIA

Dipartimento di Biologia e Biotecnologie

“Lazzaro Spallanzani”

Laurea Magistralis in Molecular Biology and Genetics

Mechanical Stress-Induced Extracellular Vesicle Release in Renal Cell Carcinoma: Implications for tumor growth and metastasis formation

Supervisor:

Prof. Federica Collino

Dr. Gaia Bianchi

Co-supervisor:

Prof. Anna Kajaste-Rudnitski

Experimental thesis by:

Anahita Sadat Deyhimi

Academic Year 2025/2026

ABSTRACT

Renal cell carcinoma (RCC) is a lethal urogenital malignancy that accounts for approximately 2% of all malignancies and arises within a highly vascularized, metabolically active microenvironment. Mechanical forces, such as matrix stiffness and solid stress, promote tumor progression through mechano-transduction and metabolic reprogramming; however, the role of mechanical stress in regulating extracellular vesicle (EV)-mediated intercellular communication in RCC remains poorly understood. Here, we investigated whether mechanical stress alters the secretion, phenotype, and functional properties of tissue-derived EVs in RCC compared with benign renal oncocytoma (RO).

Tissue specimens were obtained from 39 patients (31 with RCC and 8 with RO) to extract tissue-derived EVs before (Matrix-EVs) and after (Stress Matrix-EVs) the application of a mechanical stress. TEM confirmed the presence of intact EV-like particles within extract. NTA showed that mechanical stimulation increased EV yield. Surface-marker profiling was performed using a 37-marker panel by flow cytometry. Consistent CD9, CD63 and CD81 expression was observed in both Matrix- and Stress Matrix-EVs. In RCC samples, tissue-derived Stress Matrix-EVs were enriched with endothelial-associated markers (CD105, CD146), immune-associated markers (CD8, CD11c, CD86, CD69), and inflammatory markers (MCSP, ROR1) along with a decreased level of the epithelial marker CD326. These alterations were not observed in the comparison between Matrix- and Stress Matrix-EVs derived from RO tissues.

Functional assays showed that RCC-derived Stress Matrix-EVs induced faster wound closure and higher degrees of cell migration in both normal HK-2 and malignant 786-O cells, along with the formation of immature angiogenic networks in HMEC-1 endothelial cells. In contrast, RO-derived Stress-Matrix EVs didn't affect the migratory behavior of healthy and tumor cell lines, and caused different alterations of the angiogenetic network compared to RCC-derived EVs.

Collectively, these findings reveal that mechanical stress selectively modulates EVs release from cell populations within malignant RCC tissues, promoting cell migration and angiogenesis. As such, the present study opens to new therapeutic possibilities to prevent or stop tumor progression.

UNIVERSITÀ
DI PAVIA

Dipartimento di Biologia e Biotecnologie

“Lazzaro Spallanzani”

Laurea Magistralis in Molecular Biology and Genetics

Rilascio di vescicole extracellulari indotto da stress meccanico nel carcinoma a cellule renali: implicazioni per la crescita tumorale e la formazione delle metastasi.

Relatore:

Prof. Federica Collino

Dr. Gaia Bianchi

Correlatore:

Prof. Anna Kajaste-Rudnitski

Tesi di:

Anahita Sadat Deyhimi

Anno accademico 2025/2026

ABSTRACT (Italiano)

Il carcinoma a cellule renali (RCC) è una neoplasia urogenitale letale che rappresenta circa il 2% di tutte le neoplasie e insorge in un microambiente altamente vascolarizzato e metabolicamente attivo. Le forze meccaniche, come la rigidità della matrice e lo stress solido, favoriscono la progressione tumorale attraverso la meccano-trasduzione e la riprogrammazione metabolica. Il ruolo dello stress meccanico nella regolazione della comunicazione intercellulare mediata da vescicole extracellulari (EV) nel RCC rimane ancora poco compreso. Questo studio ha come obiettivo quello di analizzare le alterazioni in secrezione, fenotipo e proprietà funzionali di EV tissutali in presenza di uno stress meccanico, in tessuti RCC e di oncocitoma renale benigno (RO).

Campioni tissutali sono stati ottenuti da 39 pazienti (31 con RCC e 8 con RO) per estrarre EV derivate da tessuto prima (Matrix-EVs) e dopo (Stress Matrix-EVs) l'applicazione di uno stress meccanico. La microscopia elettronica a trasmissione (TEM) ha confermato la presenza di particelle integre simili a EV negli estratti. L'analisi NTA ha mostrato che la stimolazione meccanica aumenta la resa delle EV. Il profilo dei marcatori di superficie è stato valutato mediante citometria a flusso utilizzando un pannello di 37 marcatori. Matrix- e Stress Matrix-EVs hanno mostrato un'espressione comparabile di CD9, CD63 e CD81. Nei campioni di RCC, le Stress Matrix-EVs risultavano arricchite in marcatori associati all'endotelio (CD105, CD146), marcatori immunitari (CD8, CD11c, CD86, CD69) e marcatori infiammatori (MCSP, ROR1), insieme a una riduzione del marcatore epiteliale CD326. Queste alterazioni non sono state osservate nel confronto tra Matrix- e Stress Matrix-EVs derivate da tessuti di RO.

Saggi funzionali hanno evidenziato che le Stress Matrix-EVs derivate da RCC inducono una chiusura della ferita (scratch) più rapida e un aumento della migrazione cellulare sia nelle cellule normali HK-2 sia nelle cellule tumorali 786-O, insieme alla formazione di reti angiogeniche immature nelle cellule endoteliali HMEC-1. Al contrario, le Stress Matrix-EVs derivate da RO non influenzano il comportamento migratorio delle linee cellulari sane e tumorali e causano alterazioni diverse della rete angiogenica rispetto alle EV derivate da RCC.

Nel complesso, questi risultati dimostrano che lo stress meccanico modula selettivamente il rilascio di EV da popolazioni cellulari all'interno dei tessuti maligni di RCC, promuovendo la migrazione cellulare e l'angiogenesi. Questo studio apre quindi nuove possibilità terapeutiche per prevenire o arrestare la progre.

Table of contents

INTRODUCTION

1.Kidney Physiology and Renal Cell Carcinoma

1.1 Kidney Physiology and Oncogenesis

The kidneys are paired, bean-shaped organs located on either side of the posterior abdominal wall, which is protected by the lower ribs and embedded in fat and tissue beneath the lumbar muscles (1). Each kidney is enclosed in a tough fibrous capsule and is structurally divided into two main regions: the outer cortex and the inner medulla (2,3).

Each kidney contains over one million functional units called nephrons. Each consists of glomerular capillaries and an associated tubular system. Together they maintain homeostasis by regulating the fluid and chemical composition of the blood and eventually urine through three key processes: filtration, reabsorption, and secretion (2,4).

Filtration begins in the glomerulus, a cluster of capillaries packed inside Bowman's capsule, located in the cortex region, where passive hydrostatic pressure pushes the fluid and solute out of the blood through a three-layered filtration membrane (glomerular filtration barrier, GFB) to form the pre-urine. The first element of the GFB is the fenestrated endothelium, which allows blood components except the cells to pass through. The second component is represented by the negatively charged basement membrane that acts as a barrier that prevents the loss of large proteins and provides the structural support to the cellular components. Finally, the podocytes (highly specialized epithelial cells within the glomerulus) provide a final, highly selective filter thanks to the slit diaphragm, specific junctions at the level of their foot processes (2–4).

The reabsorption process occurs among four distinct tubular segments, each with unique absorptive properties. Beginning with the proximal convoluted tubule (PCT) in the cortex, where all the glucose and amino acids, along with essential vitamins, are reabsorbed to peritubular capillaries. The PCT also accounts for approximately 65% of sodium and water reabsorption by the active basolateral Na^+/K^+ pump, establishing the electrochemical gradient necessary for the secondary active transport of glucose, amino acids, and vitamins. This significant solute transport generates an osmotic gradient that facilitates the reabsorption of water. Additionally, reabsorption of urea occurs in the PCT through passive paracellular diffusion (2,5).

Following the PCT, the remaining filtrate enters the loop of Henle within the renal medulla. The descending limb facilitates significant water reabsorption via osmosis, a process made possible by a high density of aquaporins and a lack of solute permeability. As the fluid reaches the ascending limb, sodium initially moves passively down its concentration gradient in the thin segment. In the thick ascending limb (TAL), sodium, potassium, and chloride are actively reclaimed via an NKCC2 symporter. This transport is powered by the basolateral Na^+/K^+-ATPase pump, which maintains the necessary ionic gradient. Additionally, the resulting electrochemical environment drives the passive paracellular reabsorption of calcium and magnesium ions (2,6).

The final phase of tubular reabsorption takes place in the distal convoluted tubule (DCT). Here, sodium is reabsorbed through primary active transport at the basolateral membrane, which facilitates secondary active transport at the apical membrane via Na^+-Cl^- symporters and specific ion channels. In the distal portion of this segment, these transport processes are precisely regulated by the aldosterone hormone. (7)

The process of tubular secretion serves to eliminate substances that were either poorly filtered due to plasma protein binding, such as certain drugs and metabolites, or passively reabsorbed, such as urea and uric acid. The distal convoluted tubule (DCT) and collecting ducts focus on the active secretion of potassium to maintain electrolyte and hydrogen ions or chloride ions reabsorption to maintain pH balance. Ultimately, the concentration of urine is regulated by hormones such as antidiuretic hormone (ADH) (8).

Finally, urine exits into the renal calyces and renal pelvis, then travels through the ureters to the bladder for storage, and is ultimately eliminated from the body via the urethra (2,9).

Within the nephron, the proximal tubular epithelial cells (PTECs) are highly susceptible to metabolic stress due to their high energy demands, extensive amounts of mitochondria and dependence on oxidative phosphorylation to maintain solute reabsorption (10). Continuous exposure to solutes and toxins may promote a stressed cellular state that contributes to renal cell carcinoma (RCC) development (9,11).

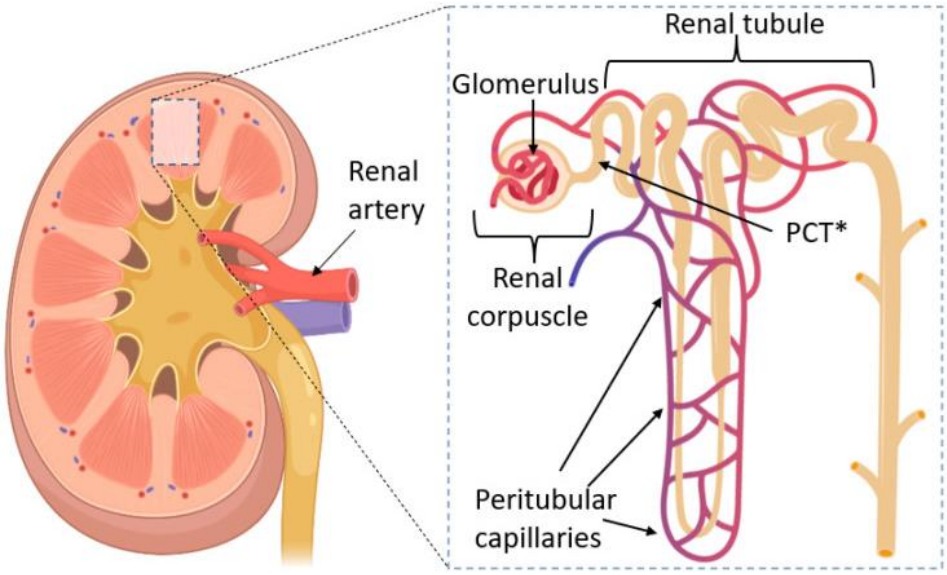

Figure 1. Anatomy of a kidney, illustrating the location of and the structure of a single nephron. The renal artery serves as the kidney's blood supply route that splits into smaller vessels called arterioles, which form bundles of vessels inside the corpuscle called glomeruli. * PCT = Proximal Convoluted Tubule, the section of the renal tubule which is directly connected to the renal corpuscle. Peritubular capillaries surround the whole tubule and transport filtered blood from the glomeruli (12).

1.2 Overview of the Epidemiology, Clinical Features and TNM classification of Renal Cell Carcinoma

Renal cell carcinoma (RCC) is considered the 14th most frequently diagnosed cancer. It is a lethal urogenital malignancy and accounts for approximately 2% of all malignancies. Notably, RCC accounts for 90% of all primary kidney cancers, with 434,000 new cases and 156,000 deaths worldwide in 2022. The male-to-female predominance is 1.5:1, with peak incidence occurring between the sixth and seventh decades of life (13,14).

RCC is known to be frequently asymptomatic, which causes most of the diagnosis to be incidentally discovered during routine abdominal imaging, such as ultrasonography and computed tomography (CT) scans. That causes a high number of patients to present with advanced tumors at the time of the diagnosis, with up to 17% of patients harboring distant metastases (15,16).

To evaluate the severity of the cancer, clinicians utilize an internationally recognized system, known as TNM staging. The assessment is based on the primary Tumor size (T), regional lymph

nodes (N), and distant metastasis(M). The T characterizes the physical dimensions and local invasion of the primary lesion. Scaling from T0 (no evidence of tumor presence), through T1-T4. The N defines regional lymph node involvement, scaling from N0-N3, with N0 as no lymph involvement. Finally, the M category distinguishes between M0 (no metastasis) and M1 (distant metastasis) (17).

Patients are further stratified for tumor grade to define the therapeutic strategy. According to the International Society of Urologic Pathologists (WHO/ISUP), RCC tumors are categorized on a scale of grade 1 to grade 4 based on the microscopic evaluation of nucleoli prominence as an indicator of how quickly a tumor is likely to grow and spread (18).

Geographically, RCC exhibits a distinct distribution, with elevated incidence rates observed primarily in Europe and North America. When examining mortality data across 27 European nations, the lowest death rates among men were documented in Luxembourg, Cyprus, and Finland, whereas the Baltic states, Czechia, and Slovakia experienced the highest male mortality rates (19)

Specific lifestyle habits can significantly contribute to increasing the occurrence of RCC, including obesity, diabetes, hypertension, smoking, and chronic kidney disease. Consequently, the most effective means to lower individual relative risk is by addressing manageable habits: maintaining a healthy weight, cessation of smoking, and limiting alcohol consumption (20).

Histologically, it divides into clear cell renal cell carcinoma (ccRCC) and non-clear cell renal cell carcinoma (non-ccRCC). ccRCC represents the most prevalent subtype, comprising approximately 80-85% of all documented cases. Approximately 40% of individuals diagnosed with ccRCC eventually progress to metastatic disease, which carries a 5-year survival rate of roughly 10%. Conversely, non-ccRCC encompasses a diverse spectrum of histopathologies. This group includes papillary RCC (pRCC), representing 10–15% of cases and arising from the epithelium of proximal convoluted tubules; pRCC is divided into type I and II, chromophobe RCC (chRCC), which accounts for roughly 5% of the cases and originates from the cortical collecting duct epithelium. Rarer subtypes include collecting duct carcinoma (CDC), renal medullary carcinoma (RMC), renal oncocytomas (RO), mucinous tubular and spindle cell carcinoma (MTSCC), in addition to tubulocystic carcinoma (TCRC), which together represent less than 1% of all RCC diagnoses (21)

1.3 Molecular Pathogenesis of RCC

While the majority of RCC cases are sporadic, hereditary forms arise due to germline mutations and epigenetic alterations, the most common of which is Von Hippel–Lindau (VHL) disease. *VHL* tumor suppressor gene is located on the short arm of chromosome 3 (3p25) (22). The Von Hippel–Lindau protein (pVHL), under normoxic (normal oxygen) conditions, functions as an E3 ubiquitin ligase that targets hydroxylated hypoxia-inducible factors (HIF-1α and HIF-2α) for polyubiquitination. This will prevent them from accumulating and dimerizing with HIF-1β and subsequent translocation to the nucleus to drive pro-angiogenic and metabolic gene expression (23).

In ccRCC, the mutation in this gene results in a constitutive stabilization and accumulation of Hypoxia-inducible factors (HIF-1α and HIF-2α), driving an aberrant "pseudohypoxic" transcriptional program that upregulates genes involved in the regulation of vascular growth and cellular metabolism, such as vascular endothelial growth factor (VEGF), glucose transporter 1 (Glut1), glycolytic enzymes, and nitric oxide Synthase (24).

Hereditary form of pRCC (HPRCC) exhibits an autosomal-dominant inheritance pattern driven by a germline mutation in the *MET* oncogene located on the long arm of chromosome 7(7q31). The *MET* gene encodes a tyrosine kinase receptor predominantly expressed on epithelial cells. Upon binding to its ligand, hepatocyte growth factor (HGF), the mutated MET receptor continuously triggers the activation of downstream intracellular signaling cascades, including RAS/ERK, PI3K, and c-Src, to collectively promote cell survival, proliferation, and suppress apoptosis, thereby facilitating renal oncogenesis specifically within the papillary Type 1 lineage. Hereditary papillary Type 2 RCC is instead driven by germline inactivation of the Fumarate Hydratase (*FH*) tumor suppressor gene at 1q42-43 (25,26)n the hereditary form of chRCC and Renal oncocytoma, the underlying driver is a germline heterozygous loss-of-function mutation in the *FLCN* gene located on 17p11.2. The condition that is clinically recognized as Birt–Hogg–Dubé (BHD) Syndrome. Under physiological conditions, this gene encodes Folliculin, a critical metabolic regulator that modulate mTORC1 complex dynamics and functions as an essential inhibitory brake on AMPK signaling (AMP-dependent protein kinase) pathway. Upon bi-allelic inactivation, this inhibitory restraint is lost, lifting the brake and constitutively activating the AMPK signaling pathway and, in many contexts, aberrant mTORC1 activation. This chronic hyperactivation falsely signals

metabolic starvation, ultimately promoting an intense, uncoordinated surge in mitochondrial biogenesis. A condition that pathologically defines oncocytic neoplasms (27)

1.4 Therapeutic Approaches to RCC

The primary approach toward localized clear cell renal cell carcinoma (ccRCC) includes partial (PN) or radical nephrectomy (RN), a surgerical approach that aims at removing a part or the entirety of the diseased kidney and its surrounding tissue (26). Conversely, Nephron-Sparing Surgery (NSS) prioritizes removing only the tumor lesion, preserving normal kidney units for patients with T1 and T2 stage tumors. For specific patient populations such as elderly, and the ones with one remaining kidney, an alternative approach includes tumor ablation that is less aggressive and can be done repeatedly; this includes Thermal Ablation (RFA and MWA), as well as Cryoablation (CA) (28,29).

For metastatic ccRCC(mccRCC), since the disease is insensitive to traditional chemotherapy, clinicians shifted their therapeutic focus toward the immune system, leading to the rise of systemic cytokine therapies in the second half of the 20th century. This approach routinely utilizes Interleukin-2 (IL-2), which activates cytotoxic T cells and boosts B cell proliferation, alongside Interferon-alpha (IFN-α), which drives the activation of natural killer (NK) cells and helper T(Th) cells (30,31)While cytokine therapy addressed patient responsiveness better than chemotherapy, it developed high levels of life-threatening risk factors, with roughly 4% of patients dying from adverse events (31).

These severe toxicities and a lack of targeting precision led to a structural shift between 2000 and 2010 toward targeted drug therapies targeting the vascular endothelial growth factor (VEGF) and mammalian target of rapamycin (mTOR) signaling pathway (32,33). The anti-angiogenesis strategy utilizes human-derived monoclonal antibodies against VEGF or multi-target small-molecule Tyrosine Kinase Inhibitors (TKIs) against the VEGFR-2 receptor on endothelial cells (34).

Sorafenib, the first marketed TKI, demonstrated higher capability to reduce tumor volume, and Sunitinib doubled median progression-free survival (PFS) to 11 months compared to IFN- α (35,36). Other subsequent TKIs with improved safety and more sensitive to refractory cases were continuously developed, including Pazopanib, Axitinib, and Cabozantinib (37).

The most recent and modern form of treatment is Immune Checkpoint Inhibitors (ICIs) therapy, which is designed to restore the cytotoxic activity of infiltrated T-lymphocytes by targeting the regulatory checkpoints that cancer cells hijack to evade adaptive immunity. These ICIs include monoclonal antibodies like Nivolumab and Pembrolizumab, which block Programmed Cell Death 1 (PD-1) receptors. Atezolizumab and Avelumab block the corresponding ligand, PD-L1, which is highly expressed on tumor cells. Additionally, Ipilimumab was developed to inhibit Cytotoxic T-Lymphocyte-Associated Protein 4 (CTLA-4), effectively preventing early-stage T-cell inactivation. (38)

As clinical treatment evolved, it became evident that a single therapy approach remains vulnerable to drug resistance and rarely produce fully durable responses. To combat drug resistance, combination therapies have gained a lot of attention. Among these, the most successful first-line standard combinations are anti-angiogenic TKIs with ICIs, precisely Axitinib-Pembrolizumab, with an extended first-line median Progression-Free Survival (PFS) of 15.1 months (39). Lenvatinib-Pembrolizumab demonstrated a superior median PFS of 23.9 months compared to Sunitinib with PFS of 9.2 months (40). Finally, Cabozantinib-Nivolumab doubled median PFS to 16.6 months and extended median overall survival to 37.7 months (41).

Other valid combinations include anti-angiogenic TKIs and targeted therapies, such as TKI Lenvatinib with the mTOR inhibitor Everolimus, or the use of two separate classes of immune checkpoint inhibitors (ICIs) such as Nivolumab (a PD-1 inhibitor) and Ipilimumab (a CTLA-4 inhibitor) (42,43)espite the therapeutic success of these advanced combinations, the inevitable emergence of drug resistance and a lack of real-time monitoring tools remain critical challenges in managing advanced ccRCC.

To address these limitations, extracellular vesicles (EVs) are positioned as promising candidates for next-generation drug delivery systems. This potential is given by their intrinsic biological advantages such as high biocompatibility, low immunogenicity, and natural capacity to cross biological barriers. Exploitation of these native transport mechanisms provides an opportunity to deliver therapeutic payloads directly to the tumor microenvironment with precision, thus providing vital clinical utility to improve treatment efficacy precisely in the context of RCC (44)

2. Classification, Biogenesis, and Physiological Function of Extracellular Vesicles (EV)

2.1 EV Classification and Characteristics

Extracellular vesicles (EVs) are heterogeneous, lipid-bilayer-bound particles secreted by all cell types into the extracellular environment and into biofluids. These vesicles carry molecular payloads from their cells of origin and therefore reflect the pathophysiological state of the parental cells. Furthermore, the distinct composition of their lipid bilayer provides structural stability and protects their cargo from enzymatic degradation (45).

Based on their biogenesis pathways, microvesicles (also known as ectosomes or microparticles) originate from the outward budding and fission of the plasma membrane and typically range from 100 to 1,000 nm in diameter (45). In contrast, exosomes are smaller vesicles, typically 30 to 150 nm in diameter, that are generated as intraluminal vesicles within multivesicular bodies (MVBs) This intracellular sorting and invagination process is orchestrated either via the classical ESCRT pathway or through ESCRT-independent lipid domains, and eventually secreted into the extracellular space upon MVB fusion with the cell membrane (45,46). Moreover, specific EV populations can arise during distinct cellular processes, such as migrasomes formed during cell migration, or apoptotic bodies generated during programmed cell death (45,47)

However, following the MISEV guidelines, relating the distinct biogenesis pathway to the extracted EVs is impossible post-isolation; therefore, the currently preferred classification is based on the EV dimensions (45).

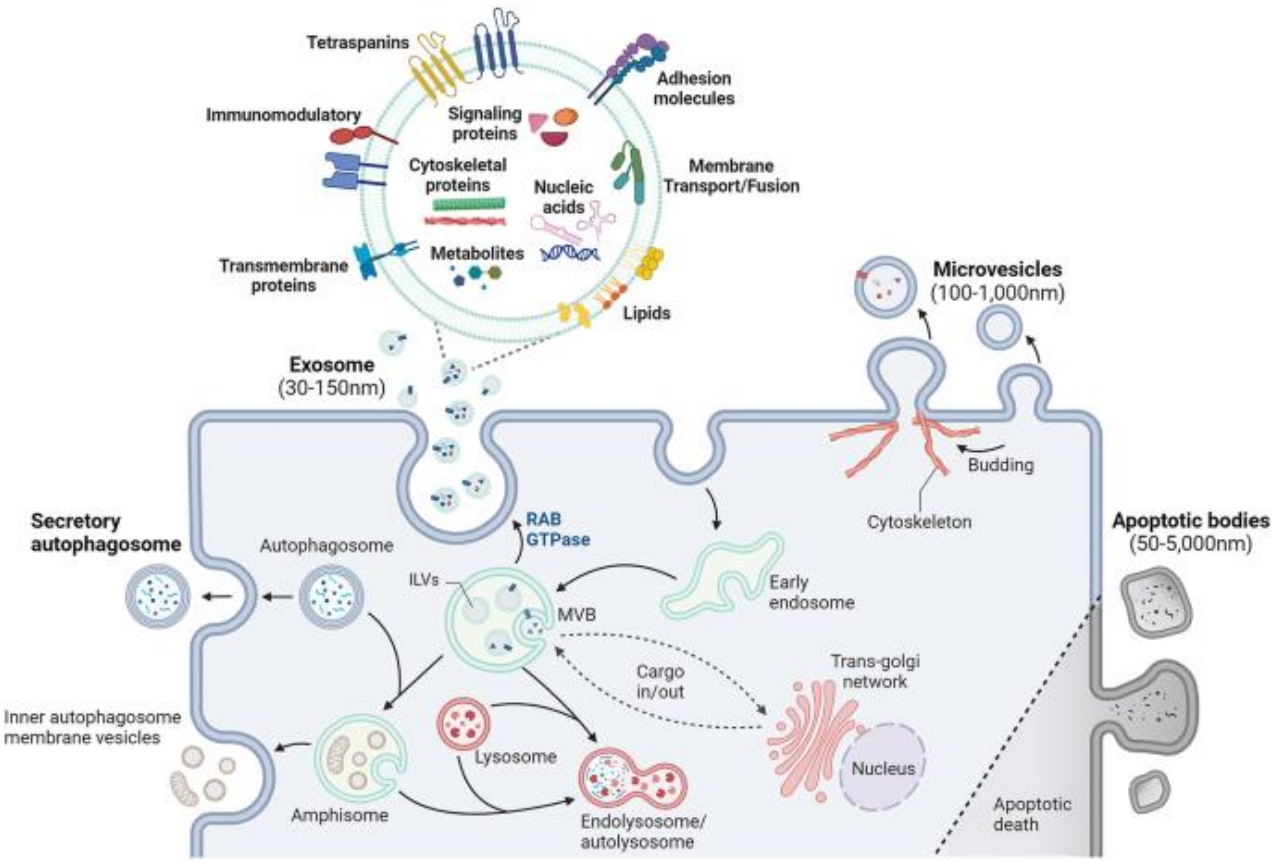

Figure 2. Schematic representation of mechanisms of extracellular vesicle (EV) biogenesis and EV cargo selection (46).

2.2 Biogenesis and Molecular Cargo

EV biogenesis is coordinated by intricate intracellular processes that give rise to either exosomes or microvesicles. Exosomal formation is coordinated through both ESCRT-dependent and -independent processes. The endosomal sorting complex required for transport (ESCRT) machinery is a cytoplasmic multisubunit complex comprising 4 distinct complexes of ESCRT-0, ESCRT-I, ESCRT-II, ESCRT-III, and the associated AAA ATPase Vacuolar Protein Sorting 4 (Vps4) Complex that promote MVB formation (48).

ESCRT-dependent pathway initiates vesicle biogenesis by the ubiquitin-binding domain of ESCRT-0, which identifies and binds to ubiquitinated proteins, leading to the sorting and segregation of these proteins into specialized endosomal membrane regions. Afterward, the proteins are handed off to ESCRT-I at the membrane compartment, followed by sequential interaction with ESCRT-II and ESCRT-III complexes. ESCRT-III polymerizes into tight spiral rings around the narrow neck of the membrane, bringing the edges closer together. Eventually, the Vps4 complex utilizes ATP hydrolysis to facilitate the vesicle pinching off the membrane to complete the formation of intraluminal vesicles (ILVs) (49).

In the ESCRT-independent pathway, the composition of secreted EVs is remarkably similar to lipid rafts microdomains enriched in cholesterol, sphingolipids, phosphatidylserine, and ceramide. Within these microdomains, neutral sphingomyelinase 2 (nSMase2) catalyzes the conversion of sphingolipids to cone-shaped lipids called ceramides, which, when tightly clustered, force the flat membrane to warp and bend inward, driving the formation of intraluminal vesicles (ILVs) within multivesicular bodies (MVBs) (50).

The proteome of the exosomes is influenced by the distinct intracellular biogenesis pathway. In the ESCRT-dependent pathway, exosome formation and multivesicular body (MVB) trafficking are regulated by ESCRT machinery. Consequently, ESCRT components and their accessory proteins such as ALIX, TSG101, HSC70, and HSP90β are commonly detected in exosomes (51). In the ESCRT-independent pathway, exosomes generated through this pathway are typically enriched in the tetraspanin proteins CD63, CD9, and CD81, along with other the plasma membrane-associated transmembrane proteins. Collectively, these molecules serve as signature markers for exosome identification.

Conversely, the biogenesis of microvesicles arises through outward budding and fission of plasma membrane, resulting from the dynamic interplay between phospholipid redistribution and cytoskeletal protein contraction. This interplay is induced by translocation of phosphatidylserine to the outer-membrane leaflet through the activity of aminophospholipid translocases, leading to loss of membrane asymmetry (52,53) Subsequently, the budding process is completed through contraction of cytoskeletal structures by actin-myosin interactions (54).

Due to their origin, MVs mainly containing cytosolic and plasma membrane-associated proteins, including tetraspanins, cytoskeletal proteins, heat shock proteins, integrins, and proteins containing post-translational modifications, such as glycosylation and phosphorylation (55).

In general, EVs carry a selective range of bioactive molecules including transmembrane and cytosolic proteins, various RNA species, and DNA fragments. in response to the physiological or pathological status of their parent cells. By this mean, EVs can modulate the physiological state of target cells through several mechanisms such as activation of intracellular signaling via receptor–ligand interactions, internalization through active uptake processes like endocytosis or phagocytosis, or direct fusion with the plasma. Through these diverse delivery mechanisms of delivery, EVs can orchestrate both local and systemic intercellular communication throughout the body (45,56).

2.3 Characteristics of Tissue-Derived Extracellular Vesicles

Tissue-derived EVs (Ti-EVs) are EVs extracted directly from tissue specimens and have been emerging as critical messengers in tumor progression and metastasis, facilitating the monitoring of physiological and pathological alterations within the localized tumor microenvironment (57).

Ti-EVs are emerging as critical messengers in tumor progression and metastasis. Thereby facilitating the monitoring of physiological and pathological alterations within the localized tumor microenvironment (57). Increasing evidence have shown the EVs isolated from tissues possess more abundant biological information and are more accurately to reflect the alteration of tissue microenvironment compared to those derived from cells and biological fluids (58).

Currently, various methods are available for isolation and purification of EVs from solid tumor tissue specimens, with two major isolation approaches being frequently used. The first approach relies on the ex vivo culture of intact tissue pieces in petri dish, which allow subsequent isolation

of the extracellular vesicles from the culture medium. While this method minimizes the risk of contamination from disrupted intracellular organelles, it is limited to fresh tissue specimens and introducing artefacts during incubation (59). The second approach is based on the enzymatic digestion of the tissue utilizing collagenase (e.g. type I and III), to extract EVs locked within the tissue. Although this method is not limited only to fresh tissue specimens, its major challenge arises when the process of extraction process, which carries a substantial risk of mechanical damage to cell membranes, which can lead to cell rupture and the co-isolation of intracellular contaminants(60,61).

However, despite the challenges, researchers aim to fully exploit the potential uses of Ti-EVs as a tool for biomarker discovery across distinct clinical stages, and more importantly for unraveling the molecular mechanisms underlying diseases (62).

2.4 EV Functional Roles in Health and Disease

EVs play a critical role in systemic homeostatic maintenance, driving critical functions such as immune regulation, neuronal communication, embryonic development, and maternal-fetal communication. In pathological contexts, such as cancer, EVs act as mediators for horizontal transfer of oncogenic signals. They promote drug resistance, immune evasion, and pre-metastatic niche (PMN) formation. Additionally, they accelerate angiogenesis by carrying cargos that can increase vascular leakiness as well as distinct molecular signatures enriched under hypoxic stress conditions. Ultimately, their baseline biochemical stability highlights their importance as physiological indicators that are uniquely suited for diagnostic and prognostic profiling. (57)

3. EVs in RCC Biology: Mechanisms and Impact

3.1. RCC-Derived EVs in the immune system

The term immune surveillance was first suggested by Frank Macfarlane Burnet and Lewis Thomas in the 1950s as a critical biological mechanism by which the body's immune system identifies and eliminates early-stage tumor cells before they progress into clinically detectable malignancies (63). To survive, cancer cells have developed sophisticated mechanisms to evade this clearance; notably, tumor-derived extracellular vesicles can exert immunosuppressive effects by suppressing the

immune system, boosting tumor immune evasion and encouraging tumor development. CD105+renal cancer stem cell-derived small EVs (sEVs) deliver Human Leukocyte Antigen-G (HLA-G), which arrests the differentiation and maturation of monocytes into functional antigen-presenting dendritic cells (DCs), consequently halting host CD3+ T cell proliferation (64).

Another immunosuppressive trait linked to sEVs in RCC is the transfer of Fas ligand (FASL), which directly binds leukocyte Fas receptors on T lymphocytes and activates cytotoxic T lymphocyte (CTL) apoptosis. Furthermore, they can stop releasing pro-inflammatory cytokines such as interleukin-2 (IL-2) and interferon-gamma (IFN-γ) from effector T cells(65). Additionally, delivering growth factor-beta 1 (TGF-beta1) to natural killer (NK) cells drives the phosphorylation of Smad2 and Smad3, which downregulates cellular degranulation and impairs overall cytolytic function (66).

Gao et al. and Diao et al. independently suggested that Heat shock protein 70 (HSP70) enforces immunological tolerance via a dual mechanism: first, is to stimulate an internal signaling pathway called STAT3 to drive massive production of myeloid-derived suppressor cells (MDSCs). (67) and second, by directly binding Toll-like receptor 2 (TLR2) on MDSCs commands them to suppress and turn off Cytotoxic T lymphocyte activity. (68)

Renal cell carcinoma (RCC)-derived small extracellular vesicles (sEVs) drive the polarization of tumor-associated macrophages (TAMs) toward an immunosuppressive M2 phenotype. By carrying circSAFB2, which targets miR-620 within recipient macrophages. result in activation of the JAK1-STAT3 signaling pathway, which leads to polarization toward the pro-tumorigenic M2 subpopulation (69). Another study found that sunitinib-resistant RCC cell-derived sEVs had greater amounts of PD-L1, which promoted the death of T cells by PD-1 and PD-L1 interactions and led to immunological tolerance (70)Therefore, to address novel therapeutic methods for metastatic RCC, it is crucial to understand these EV-mediated interactions

3.2 RCC-Derived EVs in Angiogenesis

The process of creating new blood vessels, known as angiogenesis, is crucial for eliminating metabolic waste products and providing nutrition and oxygen to the fast-growing tumor cells once a tumor exceeds a 2 mm^3 diffusion limit. Kidney renal clear cell carcinoma (ccRCC) is recognized as a highly vascularized malignancy (71). The primary genetic driver of this phenotype is

inactivation or mutation of the Von Hippel Lindau (VHL) tumor suppressor gene. This loss of function prevents the proteasomal degradation of Hypoxia Inducible Factor 1 alpha (HIF-1α), leading to its constitutive stabilization, enhanced transcriptional activity, and a pseudo-hypoxic pattern of gene expression including upregulation of vascular endothelial growth factor A (VEGF-A) and platelet-derived growth factor (PDGF) (72). Within this context, RCC-derived EVs act as mediators that deliver angiogenic signals including miRNAs and proteins to recipient cells. Moreover, in response to a hypoxic microenvironment, RCC tumor cells accelerate the secretion of EVs enriched with carbonic anhydrase 9 (CA9), a master enzyme regulator known to promote angiogenesis under oxygen deprivation (73).

Lindoso et al. demonstrated that mesenchymal stem cells (MSCs), upon internalization of extracellular vesicles (EVs) derived from renal cell carcinoma (RCC) stem cells, showed upregulation of MMP1, MMP3, and CXCR4, which effectively stimulate angiogenesis and supported tumor growth in vivo (74). In another study, CD105+ renal cancer stem cell-derived vesicles were shown to be packed with pro-angiogenic factors including VEGF, FGF2, ephrin A3, and angiopoietin 1, as well as matrix metalloproteinase mRNAs (MMP2 and MMP9) that are associated with stimulating angiogenesis (75).

3.3 RCC-derived EVs in Metastasis

Tumor metastasis requires the formation of a pre-metastatic niche at a distant site, creating a microenvironment favorable for migrating tumor cells to attach and initiate colonization. The process of tumor cell dissemination from the primary site to distant organs involves five steps: local invasion, intravasation, survival in circulation, extravasation, and colonization at the metastatic site(76). Local invasion fundamentally involves the epithelial-to–mesenchymal transition (EMT), a phenotypic shift driven by RCC-derived EVs, which can promote cancer cell migration, invasion, and lung metastasis by shuttling a long non-coding RNA called MALAT1 (77). Similarly, ccRCC-derived EVs include miR-19b-3p, a potent oncogenic miRNA with the potential to facilitate lung metastasis (78)This localized invasive reprogramming is further amplified by stromal cross-talk within the tumor microenvironment (TME). Upon internalization of EVs derived from cancer-associated fibroblasts (CAFs) by RCC cells, tumor cells were shown to upregulate critical mesenchymal markers and matrix-degrading enzymes, including fibronectin, N-cadherin, vimentin, MMP9, and MMP2 (79).

During extravasation, RCC-derived EVs deliver azurocidin 1 (AZU1), a specialized protein that effectively alters vascular endothelial cell layer permeability (80). Additionally, EVs secreted from TKI-resistant RCC cells were found to be enriched with decreased levels of miR-549a, which regulates HIF-1α expression in vascular endothelial cells, contributing to metastasis by promoting angiogenesis and enhancing vascular permeability (81). Collectively, these findings highlight the importance of RCC-derived EVs as a crucial mediator in metastasis.

3.4 Influence of RCC-derived EVs in the development of therapeutic resistance

One of the major unsolved issues in cancer biology is drug resistance in various malignancies, and renal cell carcinoma (RCC) is among the most drug-resistant cancers. Studies have shown RCC-derived EVs to play a critical role in transferring bioactive molecules from resistant cancer cells to non-resistant cancer cells, propagating the resistant behavior across the tumor, leading to therapeutic failure (82,83)

The studies in resistant cancer cells revealed high levels of AKT, which downregulates FOXO1 and FOXO3 and activates the transcription of lncARSR to be sorted in EVs. Upon uptake of these enriched EVs, lncARSR upregulates AXL and c-MET oncogenes by competitive binding to miR-34 and miR-449. Furthermore, AXL and c-MET upregulation leads to activation of the STAT3, AKT, and ERK signaling pathways, contributing to the Sunitinib-resistant trait in these cells. Because lncARSR transcription occurs downstream of the AKT pathway, it establishes a positive feedback loop that continuously drives lncARSR expression in drug-sensitive cells (83).

Another lncRNA, IGFL2-AS1, carried in EVs, induces autophagy to promote drug tolerance (84) miR-31-5p directly targets and suppresses MutL homolog 1 (MLH1), a critical part of the mismatch repair (MMR) pathway, whose downregulation induces drug tolerance and chromosomal instability. In parallel, GLUT1 increases glucose uptake and enhances glycolytic activity, both contributing to drug resistance in the recipient cell (85,86). Despite the advances in metastatic RCC (mRCC) therapies, such as TKI, ICI, and their combination, a substantial portion of patients were reported to have primary or acquired resistance to these treatments(87). Therefore, clarifying the molecular basis of this vesicle-mediated expansion of resistance is critically important for identifying novel biomarkers and therapeutic targets to improve response to treatments in RCC patients.

4. Clinical Applications of EVs in RCC

4.1 The role of extracellular vesicles in drug delivery and as therapeutic targets

Recently, extracellular vesicles (EVs) have emerged as promising vehicles for clinical drug delivery, harnessing their intrinsic biological functionalities and systemic stability.

In a study using mouse models with pancreatic ductal adenocarcinoma (PDAC), researchers demonstrated the therapeutic potential of engineered extracellular vesicles called iExosomes. These exosomes were loaded with a specific siRNA derived from fibroblasts. This approach effectively silenced the mutated KRAS transcript and prevented downstream signaling pathways. The targeting efficiency of iExosomes depends on the presence of CD47 on their surface. CD47 delivers a "don't eat me" signal to the immune system, allowing longer stability in circulation. The aggressive tumor behavior of macropinocytosis naturally increased uptake of iExosomes by tumor cells. Additionally, native surface proteins on the engineered EVs help them attach to and enter pancreatic cancer cells more efficiently (88).

Conversely, based on the natural ability of EVs to transfer bioactive cargo that favors tumor progression, researchers have focused on disrupting this intercellular communication network. To do this, they inhibit EV release either by targeting the neutral sphingomyelinase (nSMase 2) pathway or by targeting components of the ESCRT machinery. Additionally, they tried to block the downstream internalization of these pathological EVs by recipient cells (89).

However, substantial technical challenges remain a primary obstacle to clinical translation, including the need for high-yield production while maintaining critical biological activity, as well as minimizing off-target effects and immunogenicity for therapeutic safety (89). In addition, the lack of universally standardized EV isolation techniques and validated screening protocols for EV biomarkers persists (90).Focusing future efforts on these issues could accelerate the translation of laboratory-based findings to the clinic.

5. Stress in Tumor Progression

RCC is defined as a highly vascularized and immunogenic malignancy. Tumor expansion within its complex microenvironment, generates mechanical stresses, including solid stress from cell proliferation, shear stress from abnormal blood flow, and matrix stiffness resulting from extensive

extracellular matrix (ECM) remodeling (91). As these solid stresses expand, they physically compress intratumoral blood vessels, resulting in hypoperfusion and elevated interstitial fluid pressure, which ultimately impair systemic drug delivery. Through mechano-transduction, these mechanical cues are converted into intracellular biochemical signals that actively drive metabolic reprogramming, the maintenance of cancer stem cells, and key tumorigenic pathways (92)Importantly, this new mechanical landscape directly intersects with hypoxia-inducible factor (HIF) signaling, amplifying hypoxia-driven neoangiogenesis and promoting survival of aggressive cell subclones.(93)

At the cellular level, mechanical cues are detected by mechanosensitive surface molecules, including integrins, cadherins at adherens junctions, receptor tyrosine kinases, and ion channels. Among these, integrins, a widely studied family of mechanosensitive molecules, play a central role in sensing variations within the extracellular matrix. By binding ECM proteins, integrins transmit signals to focal adhesion kinase (FAK) and Rho GTPases, thereby promoting focal adhesion stabilization and activating downstream intracellular signaling cascades. Ultimately, these signals converge on multiple mechano-transduction pathways, including the YAP/TAZ cascade (94,95)

Increased microenvironment stiffness drives the activation of transcriptional regulators of Yes-associated protein (YAP) and PDZ-binding motif (TAZ), promoting their translocation to the nucleus, where they recruit TEAD (TEA domain family) transcription factors to form a functional complex (96). Upon this interaction, the YAP/TAZ/TEAD complex controls the expression of the target genes by binding to distant enhancers through DNA looping, where they’re brought into physical proximity with target gene promoters and initiate transcription. The sustained activation of YAP/TAZ in various malignancies executes a broad transcriptional program connected to cell-cycle progression, which comprises DNA replication, synthesis and repair, alongside the control of cyclins for S-phase entry, and the completion of mitosis (97). Beyond cell-cycle control, this mechanical network operates in synergy with ECM-remodeling enzymes like matrix metalloproteinases (MMPs) to stimulate the epithelial–mesenchymal transition (EMT) and induce autophagy, effectively suppressing cytotoxic immune responses to facilitate immune evasion (98). In addition, YAP/TAZ signaling contributes to metabolic reprogramming, accelerating glycolysis and glutamine metabolism to meet the bioenergetic demands of tumor progression.

In parallel to these biochemical cascades, mechanical signals can also be transmitted directly from the ECM to the nucleus. This direct mechano-transduction occurs through physical attachment via the internal actin cytoskeleton and LINC (Linker of Nucleoskeleton and Cytoskeleton) complexes, which contain nesprins and SUN-domain proteins. This physical anchoring regulates nuclear positioning and morphology, further driving aggressiveness of cancer cell behaviors such as adhesion, migration, proliferation, and cytoskeletal remodeling (97).

5.1 Stress-Induced EVs in RCC Biology: Mechanisms and Impact

In addition to biochemical signaling cascades, EV dynamics are directly regulated by mechanical stress. In particular, transmembrane integrins are stimulated by the stiffness of the extracellular matrix (ECM) and physical forces. This activation would stabilize FAK and activate the Rho/ROCK signaling cascade. This mechanical signaling disrupts ECM rigidity and cell morphology, resulting in cytosolic Hippo signaling and nuclear translocation and activation of Yes-associated protein (YAP) and transcriptional coactivator with PDZ-binding motif (TAZ) (92).

Recent evidence shows that matrix stiffening is associated with a 2-2.5fold increase in the number of exosomes. Moreover, the inhibition of this pathway by the YAP inhibitor verteporfin (VP) will entirely abolish exosome secretion. Together, these findings highlight the major contribution of matrix stiffness and mechanical forces in actively influencing EV biogenesis, secretion rates, and cargo sorting mechanisms. (99)

Once secreted into the extracellular space, extracellular vesicles act as intercellular messengers that can reshape the tumor microenvironment by transferring bioactive compounds, including metalloproteinases (MMPs) and regulatory RNAs, to recipient cells (100).This EV-mediated communication promotes oncogenic processes, such as angiogenesis, immune evasion, and the establishment of pre-metastatic niches specifically within the landscape of RCC However, the precise mechanisms underlying this mechanosensitive vesicle crosstalk remain incompletely understood, creating a gap that the present study aims to address. (92,101)

STUDY AIM

This study aims to characterize the surface marker profiles of extracellular vesicles (EVs) isolated from renal cell carcinoma (RCC) tumor tissues in the presence and in the absence of mechanical stress. By defining distinct molecular signatures that differentiate these two EV sub-populations ("matrix" versus "stress-matrix"), to see how the presence of mechanical stress changes the production of EVs from the different tumor tissue-resident cell populations.

Secondary objectives aim to study the impact of mechanical stress in the regulation of EV secretion in both malignant and benign renal tumors. Additionally, we will evaluate the functional impact of these different EV populations (“matrix” and “stress-matrix”) on recipient cells utilizing an *in vitro* RCC. To observe how mechanically-induced alterations in secreted EVs may associate with tumor-associated behaviors. Moreover, we will study whether the observed EV changes are specific to malignant tissues or represent a more general response to mechanical stimulation in renal tumors.

Collectively, these objectives attempt to bridge the gap between mechanical stress and intercellular communication in RCC and lay an essential foundation for the translation of mechanosensitive vesicle signatures into clinically diagnostic and prognostic tools.

MATERIALS AND METHODS

1.Patient Recruitment.

This study recruited 39 patients, all of whom provided written informed consent prior to inclusion. Whitin this cohort, 31 patients were diagnosed with renal cell carcinoma (RCC) presenting tumor grade higher than 2, while the remaining 8 patients were classifies as having renal oncocytoma (RO). The patients' surgical operation consisted of either partial or total nephrectomy. Following resection, the surgical specimen was transferred to the Pathology Unit (U.O.C. of Anatomo-Pathology) at IRCCS Ca Granda, where a piece of tumor specimen was harvested for biobanking and extracellular vesicle (EV) extraction. All specimens were immediately immersed in 50ml propylene tubes containing HypoThermosol® FRS supplemented with 1% penicillin/streptomycin and maintained on ice at 4°C until processing.

Table 1- Clinical characteristics of the recruited patients.

Parameters		Recruited patients (n=39)
Age (yr), mean (SD)		64.2 (12.6)
Sex, n (%)		
	Male	30 (76.9)
	Female	9 (23.1)
Type of nephrectomy, n (%)		
	Partial	24 (61.5)
	Total	15 (38.5)
Tumor size (cm), mean (SD)		4.6 (1.8)
Tumor grade, n (%)		
	2	19 (48.7)
	3	5 (12.8)
	4	4 (10.3)
	N/D	11 (28.2)
Tumor stage, n (%)		
	pT1a	15 (38.5)
	pT1b	11 (28.2)
	pT2a	2 (5.1)
	pT2b	0 (0.0)
	pT3a	8 (20.5)
	pT3b	1 (2.6)
	N/D	2 (5.1)
Histology, n (%)		
	RCC	31 (79.5)
	RO	8 (20.5)
Cancer subtype, n (%)		
	clear cell	24 (61.5)
	papillary	4 (10.3)
	chromophobe	3 (7.7)
	N/D	8 (20.5)
Metastases, n (%)		
	positive	3 (7.7)
	negative	27 (69.2)
	N/D	9 (23.1)
Follow up, n (%)		
	No Evidence of Disease	19 (48.7)
	Metastases	2 (5.1)
	Dead	2 (5.1)
	N/D	16 (41.0)
Relevant comorbities, n (%)		
	yes	17 (43.6)
	no	22 (56.4)

2. Isolation of Tissue EVs.

Harvested tissues were washed with PBS and weighed prior to subdivision. For biobanking, fragments of 200-300 mg were transferred into 1ml CryoStore® CS10 cryopreservation solution and stored at –80 °C. The remaining tissue (150-200 mg) was placed in a petri dish and gently minced into small pieces and then it subjected to enzymatic treatment with RPMI containing 40 U/ml DNase I (Catalog No. 11284932001; Roche Diagnostics) and 2 mg/ml collagenase D (Catalog No. 11088866001; Roche Diagnostics). The digestion was performed in a total volume of 2 mL, divided between two wells of a 24-well plate (1 mL per well), and incubated for 30 minutes at 37°C with gentle agitation every 10 minutes.

Following incubation, the treated tissue pieces were transferred onto a 70 µm cell strainer and washed 10 times with 0.1 µm-filtered PBS to collect matrix-EVs into 50ml polypropylene tubes. The cell strainer was then placed on a clean 50ml Falcon tube, where mechanical stress was applied to the tissues for 10 min while washing with 0.1 µm-filtered PBS to obtain stress matrix-EVs. The resulting filtrates were centrifuged at 300 × g for 10minutes at 4 °C to pellet the cells.

The EV-containing supernatants were then passed through a 40 µm cell strainer and centrifuged at 2,000 × g for 20 min at 4 °C to remove residual cell debris. The samples were subsequently concentrated using 100 kDa molecular weight cut-off (MWCO) filters at 3,000 × g for 15 minutes at 4 °C, following two washes with 0.1 µm-filtered PBS to concentrate tissue-derived EVs while removing low-molecular-weight contaminants, yielding an < 500 µL EV-enriched concentrate. Finally, 1% DMSO was added to the concentrates, which were then aliquoted for nanoparticle tracking analysis (NTA), electron microscopy (EM), and subsequent functional assays and stored at –80 °C. A comprehensive schematic overview of the workflow is presented in *Figure 1.*

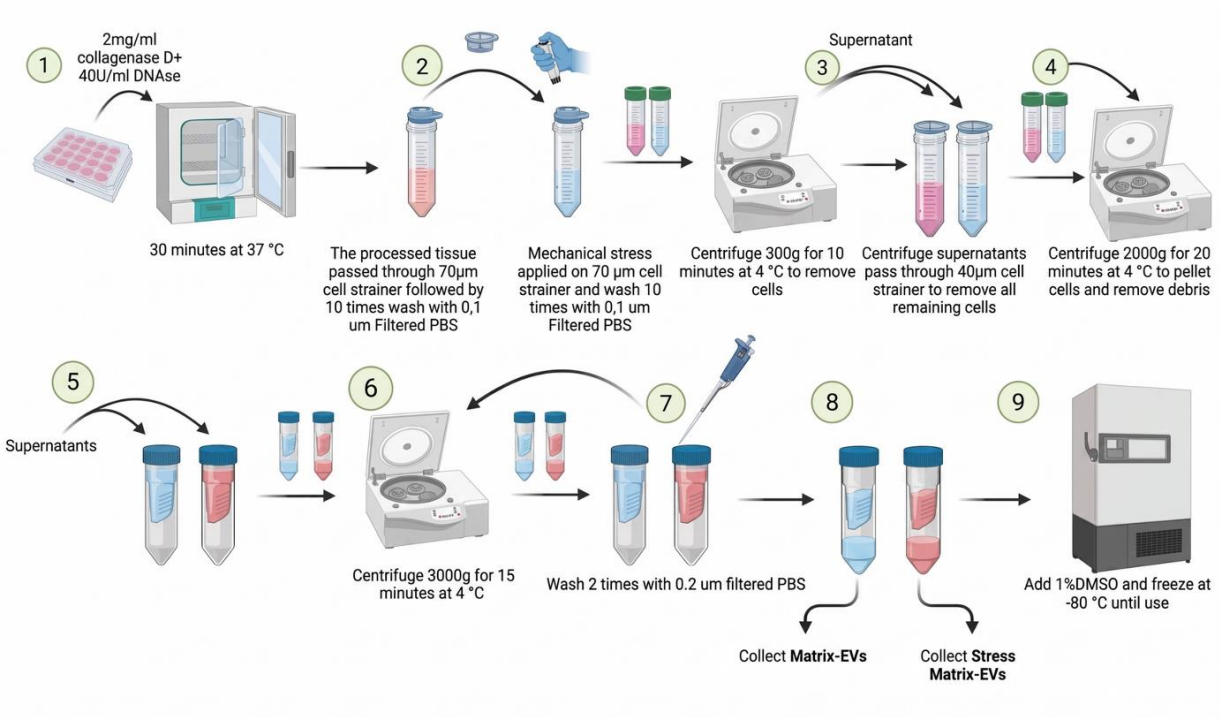

Figure 3. Schematic overview of Matrix-EVs and Stress Matrix-EVs extraction from tumor tissue. Image created with BioRender.

3.Nanoparticle Tracking Analysis (NTA)

To measure EV concentration, a 1:500 dilution was prepared in PBS 0.1 µm and measured by NTA using a NanoSight (Nanosight, UK). The sample was loaded into the chamber using a syringe pump, and three sequential flow rates of 1000 µL/min, 300 µL/min, and 30 µL/min were used. Three sequential 60-second videos were then recorded at a constant flow rate of 30 µL/min to characterize particle concentration and size distribution.

4. Transmission Electron Microscopy (TEM) of Tissues and Tissue-Derived EVs

TEM examination of the tissue-derived extracellular vesicles and tumor tissues, including those under stress, was conducted through direct fixation of the specimens using 4% paraformaldehyde (PAF), 0.25 M HEPES, and 2.5% glutaraldehyde (Sigma-Aldrich). The specimen was analyzed utilizing a Tecnai G2 transmission electron microscope (FEI Company) functioning at 100 kV. Image acquisition was enabled by a Veleta digital camera (Olympus Soft Imaging System).

5.EV pool preparation

To establish the malignant experimental group for functional assays, matrix- and stress matrix-EVs derived from two Grade 2 and two Grade 3 Renal Cell Carcinoma (RCC) specimens were pooled at equal representation of both histological grades. Four Renal Oncocytoma (RO) samples were also pooled to test matrix- and stress matrix-EVs function. The pooled EVs were then aliquoted into assay-specific volumes based on concentrations determined by the NTA readouts. Finally, to ensure reproducibility, each pool was tested in duplicate across two independent experimental runs for each functional assay.

6.Surface Markers Characterization through Flow Cytometry

For the characterization of tissue-derived extracellular vesicles (tissue-EVs), cell surface phenotyping was executed using the MACSPlex exosome kit (Miltenyi Biotec, Bergisch Gladbach, Germany) in accordance with the protocol provided by the manufacturer. Briefly, 5×10^9 particles were suspended in MACSPlex buffer to achieve a final reaction volume of 120 µL. The samples were subsequently incubated overnight at 4°C with fluorescein isothiocyanate (FITC)- and phycoerythrin (PE)-labeled capture beads pre-coated with monoclonal antibodies targeting 37 distinct exosomal surface epitopes, alongside two isotype controls (REA and IgG1). As a negative control, capture beads were incubated in the buffer solution completely free of EVs. The next day, the resulting bead-EV complexes were isolated via centrifugation at 3,000 × *g* for 5 minutes and then labeled with an APC-conjugated detection antibody cocktail directed against the primary tetraspanins CD9, CD63, and CD81. Following sequential washing steps, flow cytometric analysis was performed using a BD FACSCanto II system (Becton Dickinson, San Diego, CA, USA). Background and non-specific signals were eliminated by subtracting the median fluorescence intensity (MFI) of both the blank buffer negative control and the isotype controls from each marker's individual MFI within the same run. These background-corrected marker MFIs were subsequently normalized against the average total APC signal of the respective sample. Data processing and evaluation were carried out using FlowJo software version 10.8.1 (Becton Dickinson, San Jose, CA, USA).

7. Surface Tetraspanins Characterization through Leprechaun

To achieve a higher-resolution evaluation of tetraspanin expression profiles—specifically their co-expression patterns on individual vesicles—tissue-derived extracellular vesicles (tissue-EVs) were characterized on the Leprechaun platform using the specialized tetraspanin kit in accordance with the manufacturer's protocol. Briefly, tissue-EVs were loaded onto microarray chips functionalized with tetraspanin to capture antibodies and incubated for 16 hours. The following day, the chips underwent sequential washing steps before the immobilized tissue-EVs were stained with a cocktail of fluorophore-conjugated tetraspanin detection antibodies for 1 hour at room temperature in the dark.

8.Cell culture and maintenance

8.1 HK-2 cell line (human kidney 2)

The immortalized human proximal tubule epithelial cell line was purchased from CliniSciences (Catalog #T0011004) under the research project RC23/2250. Cells were maintained and grown in Keratinocyte-SFM (1X) Serum Free Medium (10724-011, Lot #3047845, Gibco) supplemented with 2% Fetal Bovine Serum (ECS5000L, Lot #EUS5307022, Euro clone). Cultures were incubated at 37°C, 5% CO2. Cells were passaged every 3 to 4 days upon reaching 70-80% confluency by disaggregating the adherent layer into a single-cell suspension using a 1X Trypsin-EDTA Solution (T4174, Sigma-Aldrich).

8.2 786-O cell line

The human renal clear cell carcinoma (ccRCC) cell line was purchased from Cytion (Catalog# 300107). Cells were maintained and grown in RPMI-1640 MEDIUM, 100 mL SIGMA, supplemented with 10% Fetal Bovine Serum (ECS5000L, Lot #EUS5307022, Euroclone). Cultures were incubated at 37°C, 5% CO2. Cells were passaged every 3 to 4 days upon reaching 70-80% confluency by disaggregating the adherent layer into a single-cell suspension using a 1X Trypsin-EDTA Solution (T4174, Sigma-Aldrich).

8.3 HMEC-1 cell line

Human Microvascular Endothelial Cell Line was purchased from Cytion (Catalog#304064). Cells were maintained and grown in EndoGro medium (Sigma-Aldrich, Catalog# SCME004) supplemented with 2% Fetal Bovine Serum (ECS5000L, Lot #EUS5307022, Euroclone). Cultures were incubated at 37°C, 5% CO2, and cells were passaged every 2 to 3 days upon reaching 70-80% confluency by disaggregating the adherent layer into a single-cell suspension using a 1X Trypsin-EDTA Solution (T4174, Sigma-Aldrich).

9.Scratch Assay

HK-2 cells were seeded in 24-well plates at 1 x 10^5cells per well in 500 µL Keratinocyte-SFM supplemented with 2% FBS a. For or 786-O cells the seeding density was set at 1.2 x 10^5 cells in RPMI-1640 medium supplemented with 10% FBS. Both cell lines were subsequently incubated at 37 °C in 5% CO2 until confluency was reached. A sterile 1000 ul pipette tip was then used to make a linear scratch across the center of each well. Wells were washed with PBS to remove detached cells and debris, and the medium was replaced with 500 µl serum-free KSFM for HK-2 and RPMI+0.1% EV-depleted FBS for 786-O. Using a Leica time-lapse microscopy system, Scratches were imaged at T0 before any treatment to establish the baseline area. Cells were then treated with 50,000 EV per cell from the relevant pools, prepared in PBS with 1% DMSO: Matrix-EVs and Stress Matrix-EVs from RCC and benign oncocytoma (RO), and PBS containing 1% DMSO as the vehicle control. Further images were acquired at 6 hours, 24 hours, and 48 hours to monitor wound closure. Fiji software was used to measure the wound area, and the percentage of closure was calculated using the following formula: Wound closure (%) $=A_0\text{-}A_t / A_0$ * 100

10.Migration Assay

HK-2 cells were plated at 2×10^4 on the upper chamber of a 8µm-porous transwell insert in 200 µL of KSFM, whereas the lower chamber received 700 µL KSFM medium. Specific EV pools were administered in the upper chamber at the identical standardized dose of 50,000 per cell that were prepared in PBS containing 1% DMSO, with the exception of the positive control, which received KSFM supplemented with 2% FBS in the lower chamber compartment

In a separate 24-well plate, 786-O cells were seeded at 2×10^4 in 200 µL of RPMI supplemented with 2% FBS-EV depleted in the upper chamber. and 700 µL RPMI+2% FBS EV-depleted was added to the lower chamber. subsequently, specific EV pools were administered at a standardized dose of 50,000 particles per cell. The treatments were prepared in PBS with 1% DMSO and included six EV pool conditions apart from the positive control where RPMI+10%FBS was added to the lower chamber.

Following 24 hours of incubation at 37 °C in 5% CO2, culture medium was removed from both cell lines, and the inserts were gently washed with PBS. Cells were fixed by adding 700 µl of cold methanol to the lower chamber and incubated at 4 °C for 15 minutes. The inserts were then washed twice with PBS, and non-migrated cells on the upper surface of the transwell membrane were carefully removed, followed by swabbing with a cotton swab.

After two additional washes with PBS, 700 µl of crystal violet was added beneath the inserts to be incubated at room temperature for 20 min to stain the migrated cells. The inserts were then washed four times with PBS, and the upper surface of the transwell membrane was gently swabbed again to remove non-migrated cells. Following a final wash, the inserts were left at room temperature and allowed to dry out.

Images were then acquired using a Leica time-lapse microscopy system. Captured 4 images at 10X magnification and 1 image at 5X magnification per insert. The quantifications were then evaluated utilizing ImageJ/FIJI software.

11.Angiogenesis Assay

Matrigel® (Corning, Lot #07825004) was thawed on ice at 4°C overnight. To prevent premature polymerization, 1000 µL pipette tips and a 24-well plate were pre-chilled at 4°C. Each well was coated with 500 µL of Matrigel, which was distributed on ice by tilting the plate; the excess was then removed to leave a thin coating. The plate was incubated at 37°C in 5% CO_2 for one hour to allow for complete solidification.

HMEC-1 cells were seeded at a density of 8×10^4 in 400 µL of serum-free EndoGro basal medium. For the physiological positive control2% FBS and kit supplements (Sigma-Aldrich, Cat# SCME004-S) were added to the basal medium. Following seeding, EV pools were administered

at a standardized dose of 50,000 particles per cell. Finally, images were acquired at 4, 6, and 24 hours post-treatment. A Leica time-lapse microscope system was then used to obtain the images. Each well was captured four times at 10X magnification. After that, the quantifications were assessed using ImageJ/FIJI software.

12.Statistical Analysis

Quantitative values are reported as mean ± SEM. Data distribution was assessed using the Shapiro–Wilk test. For comparisons between two independent experimental groups, either an unpaired t-test or the non-parametric Mann–Whitney test was performed, depending on data normality. Paired data were analyzed with paired t-test or the non-parametric Wilcoxon signed-rank test depending on the data distribution. Statistical analyses and data visualization were carried out using GraphPad Prism version 9.5.0 (GraphPad Software, San Diego, CA, USA).

RESULTS

1.Characterization of EVs revealed that mechanical stress drives a higher yield of EVs from tumor tissue while preserving their morphology.

Transmission electron microscopy (TEM) analysis has confirmed that EVs maintain a consistent morphology across both isolation procedures of matrix-derived *(Fig. 4A)* and mechanically stimulated *(Fig. 4B*) extractions. The isolated particles exhibited the rounded morphology and size characteristic of extracellular vesicles. Crucially, TEM imaging verified the integrity of cell membrane following the application of mechanical stress *(Fig. 4C)*, indicating that EVs were effectively extracted from the tissue, rather than randomly released as a consequence of cell rupture. Further characterization via Nanoparticle tracking analysis (NTA) revealed that mechanical stimulation resulted in a significantly higher concentration of isolated EVs compared with their matrix-derived counterparts. (*$p<0.05$*; *Fig. 4D*). while the average vesicle size distribution remained essentially identical and overlapping between both extraction methods *(Fig. 4E)*.

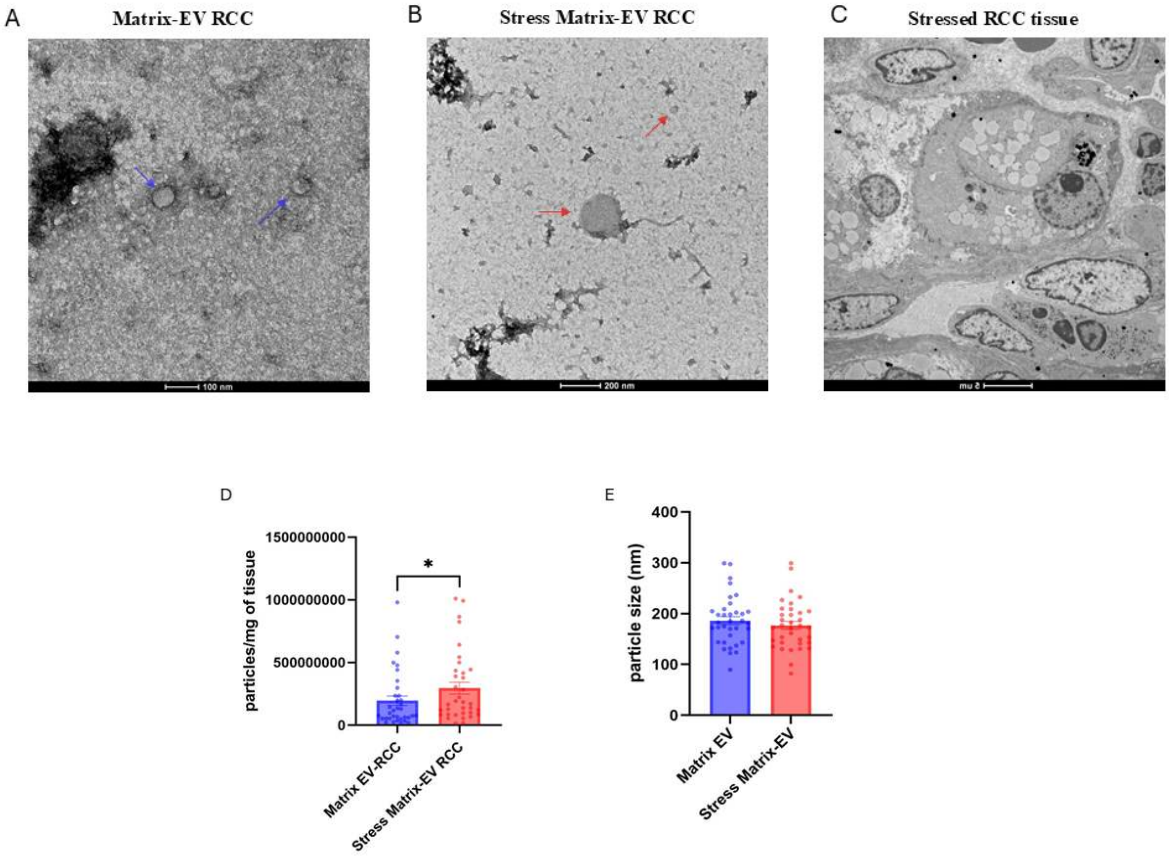

Figure 4 – Characterization of EVs from tumor tissues using TEM and NTA.
(A) TEM image showing Matrix-EVs with typical rounded morphology isolated from RCC tissues (indicated by dark blue arrows). **(B)** TEM image showing Stress Matrix-EVs with typical rounded morphology isolated from RCC tissues (red arrows). **(C)** TEM image of an RCC tissue section showing intact cells following application of mechanical stress. **(D)** NTA particle quantification of tumor matrix-EV (n = 35) and tumor stress matrix-EV (n = 35) samples. Particle number is expressed per milligram (mg) of processed tissue. **(E)** NTA size profiling of extracted EVs (n = 35). $p < 0.05$. Statistical analysis was performed using paired t-test or Wilcoxon matched-pairs signed-rank test.

2.Surface tetraspanin profiling reveals a highly stable expression pattern across Matrix-and Stress Matrix-EVs

The surface molecular profiling across both Matrix-EV and Stress Matrix-EV demonstrated the stable expression of classical tetraspanins expression remain consistent across samples and is unaffected by mechanical stress (n = 33) *(Fig. 5A).* In particular, in both EV groups, CD9 was identified as the most abundantly expressed marker with an average MFI of 10503 and 5998 on Matrix- and Stress Matrix-EVs, respectively, followed by a CD63 and CD81. Notably, no statistically significant differences were observed between the two groups.

To further strengthen these findings, Leprechaun single-vesicle analysis was performed on EVs derived from three independent RCC patients, comparing baseline Matrix-EV *(Fig. 5B)* and Stress Matrix-EV *(Fig. 5C).* Consistent with the previous results, the overall fraction of EVs expressing specific markers and their colocalization patterns remained stable under stress conditions. In particular, CD9 and CD63 marker were confirmed as the main tetraspanins in all conditions. Tetraspanin co-localization was restricted to a smaller EV subset, with double-positive vesicles accounting for 13% of the total population in tumor Matrix-EVs and 5% in tumor Stress Matrix-EVs. Triple-positive EVs constituted the least fraction, accounting for 1.14% , and 2.55%, in Matrix- and Stress Matrix-EVs respectively.

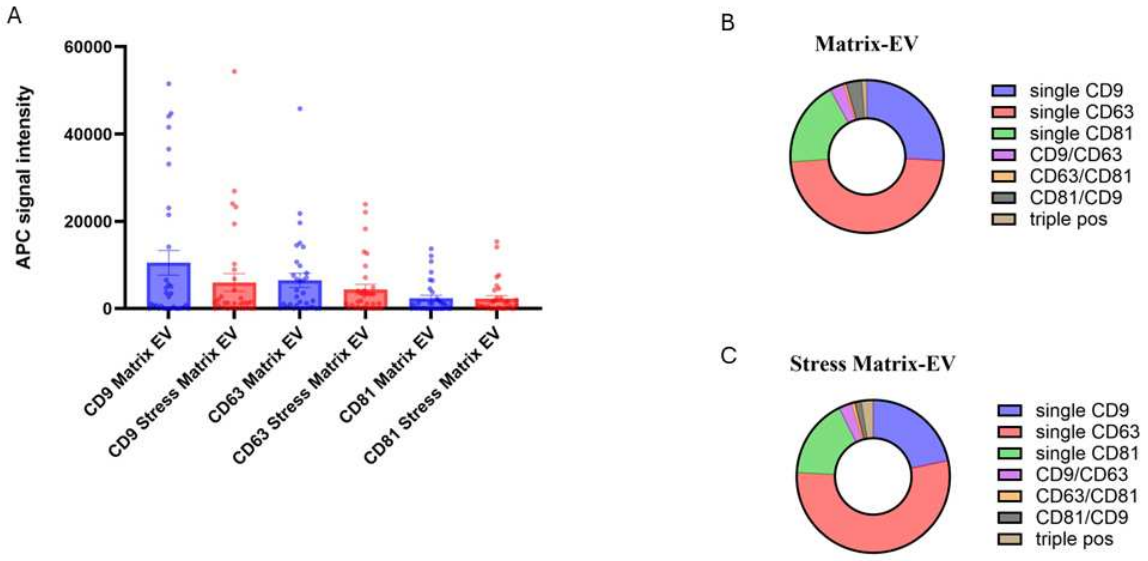

Figure 5. Surface characterization of tetraspanins in Matrix- and Stress Matrix-EVs.
(A)Tetraspanin profiling of (CD9, CD63,CD81) tetraspanins in Matrix and Stress Matrix-EVs (n=33 per condition) measured via MACSplex at flow cytometry. (B-C) Donut charts showing the distribution of single, double and triple tetraspanin expression single-vesicles quantified via Leprechaun (n=3 per condition)

3.Mechanical stress induces distinct surface marker alterations in malignant renal cell carcinoma compared with benign oncocytoma cohorts.

To evaluate the relationship between mechanically induced EVs and tissue malignancy, a comprehensive profiling of a 37-surface-marker panel was conducted on the RCC and RO patient cohort.

In the RCC patients' cohort (n=27), a general increase in marker expression on the surface of Stress Matrix-EVs compared to Matrix-EVs (*Fig. 6A*) was observed. In particular, the application of mechanical stress on RCC tissues resulted in an enrichment of immune-derived EVs, as indicated by the increased levels of CD8 ($p < 0.05$), CD11c ($p < 0.05$), CD86 ($p < 0.01$), and CD69 ($p < 0.05$) on Stress Matrix-EVs compared with Matrix-EVs. Inflammatory markers MCSP ($p < 0.05$) and ROR1 ($p < 0.01$) were also elevated in Stress Matrix-EVs relative to Matrix-EVs. Additionally, stressed tissues yielded the isolation of a higher proportion of endothelial-derived EVs, as demonstrated by the increased signal intensity of CD105 ($p < 0.05$) and CD146 ($p < 0.01$) in the corresponding EV populations. Conversely, a statistically significant decrease in epithelial-derived EVs expressing CD326 was detected under mechanical stress conditions ($p < 0.05$, *Fig. 6B*).

On the other hand, the analysis within the benign renal oncocytoma (RO) patient cohort (n = 6) revealed a distinct response to mechanical stress compared with the RCC cohort. Indeed, mechanical stress induced no significant alterations in immune, inflammatory, or endothelial markers. However, the epithelial marker CD326 exhibited the same decrease pattern observed in the RCC cohort ($p < 0.05$; *Fig. 7*), suggesting that epithelial down-regulation represents a more generalized tissue-level response of renal structures to mechanical stress.

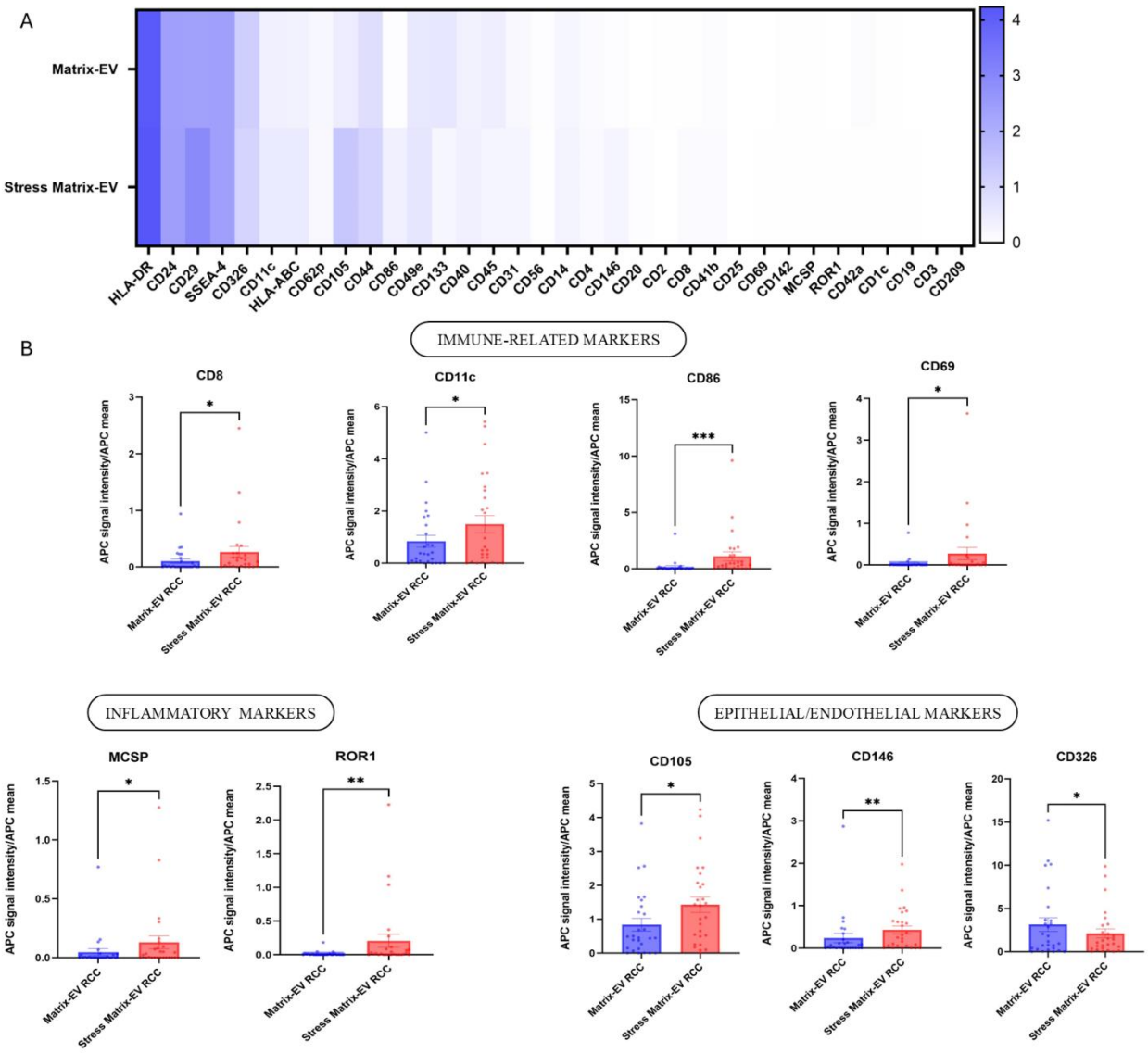

Figure 6. Differential expression of immune-related, inflammatory, and epithelial/endothelial surface markers across Matrix-EVs and Stress Matrix-EVs in RCC.

(A) Heatmap plot representing the expression profile of 37 surface markers on RCC-derived Matrix-EVs and Stress Matrix-EVs quantified via MACSPlex analysis using flow cytometry (n = 27). (B) Bar graphs showing the individual expression levels of significantly altered markers across distinct functional classifications, comparing Matrix-EV (blue bars) and Stress Matrix-EV (red bars) cohorts in RCC patients (n = 27): *Immune-Related Markers* (CD8, CD11c, CD86, CD69); *Inflammatory Markers* (MCSP, ROR1); and *Epithelial/Endothelial Markers* (CD105, CD146, CD326). Statistical analysis was performed with a Wilcoxon matched-pairs signed-rank test; * $p < 0.05$, ** $p < 0.01$.

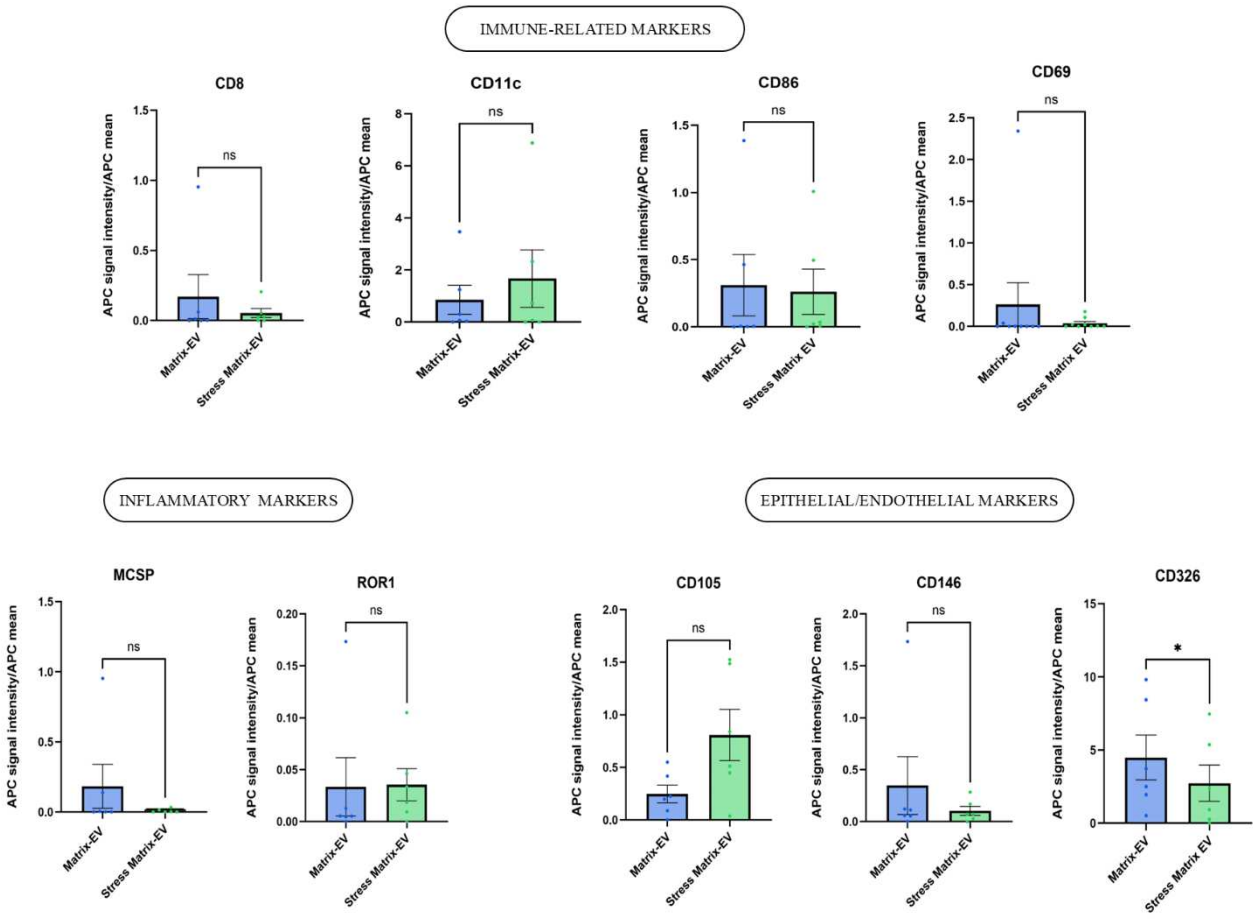

Figure 7. Evaluation of immune-related, inflammatory, and epithelial/endothelial surface markers across Matrix-EVs and Stress Matrix-EVs in the benign RO cohort.

Bar graphs showing the individual expression levels of surface markers across distinct functional classifications, comparing Matrix-EV (blue bars) and Stress Matrix-EV (green bars) counterparts in the RO patient cohort (n = 6): *Immune-Related Markers* (CD8, CD11c, CD86, CD69); *Inflammatory Markers* (MCSP, ROR1); and *Epithelial/Endothelial Markers* (CD105, CD146, CD326). Statistical analysis was performed with a Wilcoxon matched-pairs signed-rank test. *ns*=not significant, *p<0.05

4. RCC Stress Matrix-EVs Accelerate Wound Closure in HK-2 and 786-O Cells Compared with Matrix-EVs

To evaluate the functional impact of Matrix-EVs and Stress Matrix-EVs on cell proliferation and motility, a wound healing assay was performed on the normal proximal tubular cell line HK-2 and the human renal cell carcinoma cell line 786-O.

In the HK-2 cell line scratch closure under the different experimental conditions was monitored over 48 time period (*Fig. 8*). While no significant differences were observed at the 24h timepoint. By 48 hours, HK-2 exposed to Stress Matrix-EVs from RCC tissues reached 76.7% wound closure exhibiting a statistically significant higher closure rate compared to cells stimulated with RCC Matrix-EVs, showing a final closure of 58.6% ($p<0.05$) On the other hand, no statistically significant difference in gap closure was found at 48 hours in HK-2 stimulation with either Matrix- or Stress Matrix-EVs from benign RO tissues.

Owing to the tumor origin of the 786-O cell line, it exhibits a higher proliferation rate and therefore scratch closure occurs much faster, with wounds completely closing by the 48-hour timepoint. Consequently, the scratch area for this cell line was measured at 8 and 24hours (*Fig. 9A*). At 24 h, RCC Stress Matrix-EVs induced 87.17% scratch closure, compared to 68.81% closure in RCC Matrix-EVs ($p < 0.01$; *Fig. 9B*). Consistently with what we observed in HK-2 cells, no significant difference in closure at 24 h was observed between Stress Matrix-EVs and Matrix-EVs derived from RO tissues (*Fig. 9C*).

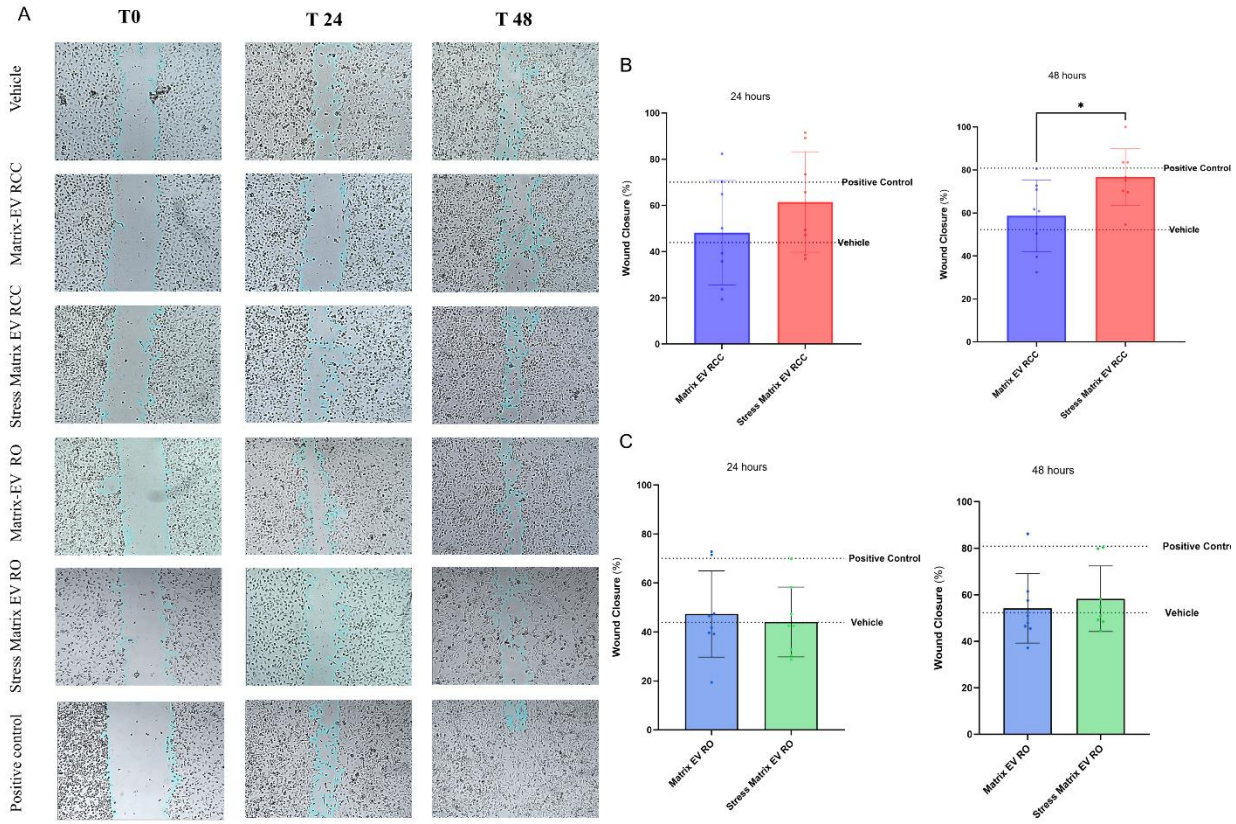

Figure 8. HK-2 cell wound closure rates under Matrix-EV versus Stress Matrix-EV from RCC and RO tissues over time.

(A) Microscopic evaluation of HK-2 cells wound closure at 0, 24 and 48 hours following treatment with test conditions. (Vehicle, Matrix-EV RCC, Stress Matrix-EV RCC, Matrix-EV RO, Stress Matrix-EV RO, and Positive control). Blue lines outline the migrating cell borders. Field of view = 1740 × 1305 µm. images were captures via Leica time-laps microscopy and analyzed using the Wound-healing size tool plugin in Fiji (ImageJ). (B) Wound closure rate in HK-2 cell line treated with RCC Matrix-EV and Stress Matrix- EV at 24 and 48 hours. A statistically significant increase in closure was observed in the stress condition at 48 hours (76.71% and 58.65%, respectively) (C) Wound closure rate in HK-2 cell line treated with RO Matrix-EV and Stress Matrix-EV at 24 and 48 hours. Statistical analysis was performed using an unpaired t-test. (n = 2 EV pools). Data are presented as mean ± SEM*; *p* <0.05.

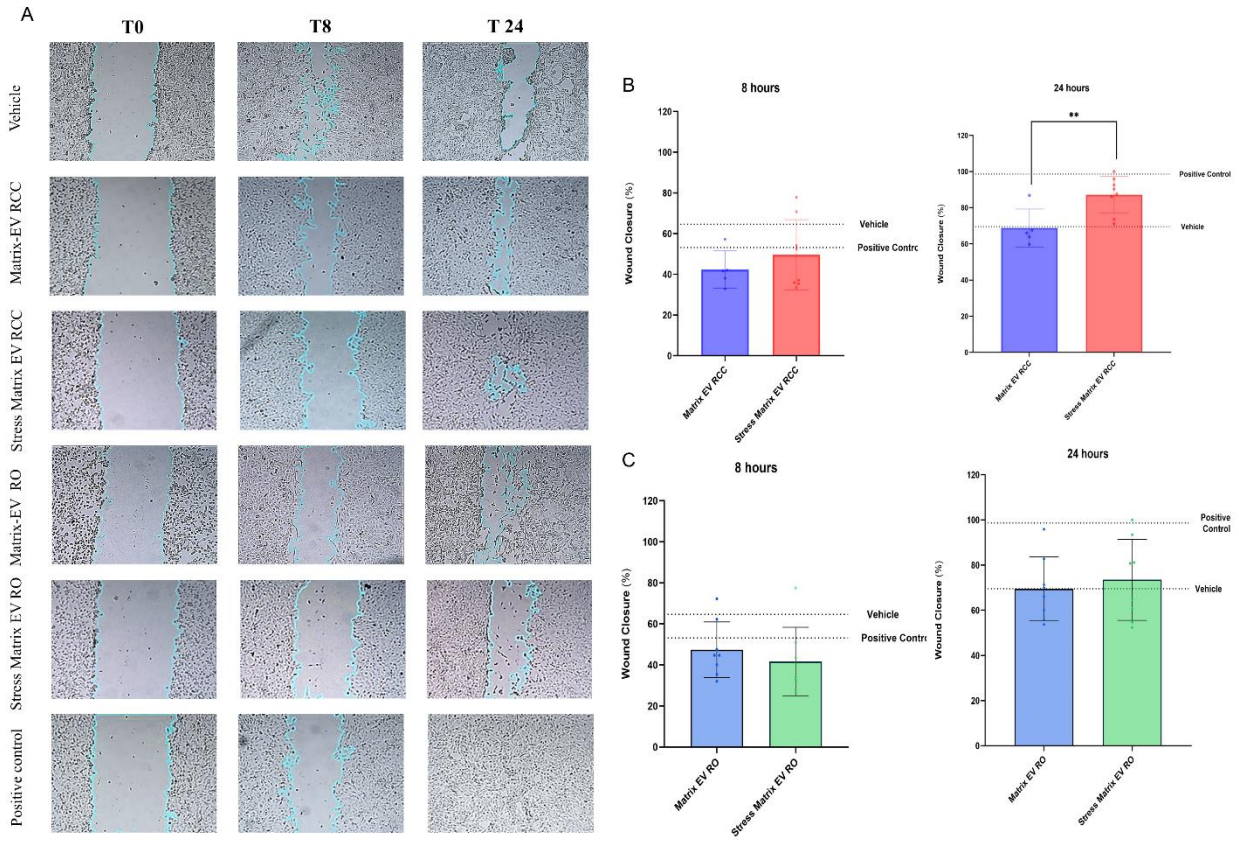

Figure 9. Bar graphs comparing 786-O cell wound closure rates under Matrix-EV versus Stress Matrix-EV conditions over time.

(A)Microscopic evaluation of 786-O cells wound closure at 0, 8 and 24 hours following treatment with test conditions. (Vehicle, Matrix-EV RCC, Stress Matrix-EV RCC, Matrix-EV RO, Stress Matrix-EV RO, and Positive control). Blue lines outline the migrating cell borders. Field of view = 1740 × 1305 µm. images were captures via Leica time-laps microscopy and analyzed using the Wound-healing size tool plugin in Fiji (ImageJ). (B) Wound closure rate in 786-O cell line treated with RCC Matrix-EV and Stress Matrix-EV at 8 and 24 hours. A statistically significant increase in closure was observed in the stress condition at 24 hours (87.17% and 68.81%, respectively) (C) Wound closure rate in 786-O treated with RO Matrix-EV and Stress Matrix-EV at 8 and 24 hours. Statistical analysis was performed using an unpaired t-test. (n = 2 EV pools). Data are presented as mean ± SEM]; **p<0.01

5. RCC Stress Matrix-EVs Promote Migration of HK-2 and 786-O Cells Compared with RCC Matrix-EV

To further investigate the specific role of Matrix-EVs and Stress Matrix-EVs in driving cell motility, a transwell migration assay was performed on both HK-2 and 786-O cell models over a 24-hour incubation window with an 8 μm porous membrane barrier.

Quantitative analysis revealed that the HK-2 cell line treated with RCC Stress Matrix-EVs exhibited the significant accelerated rate of migrated cells after positive control, yielding a minimum count of 120. Whereas, the RCC Matrix-EV treatment resulted in 85 migrated cell counts. (*Fig. 10B)* Additionally, a lower magnitude was observed between the migrated cells counts following the treatment with RO Stress Matrix-EVs and RO Matrix-EV, which yielded an average of 79 and 61, respectively. (*Fig. 10C*)

In parallel, this stress-induced effect was further reproducible in the 786-O cell line which exhibited an overall higher baseline of migrating cells compared to the HK-2 line, especially 786-O treated with RCC Stress Matrix-EV, demonstrated an increase significant in migration relative to the RCC Matrix-EV with an average count of 351, and RCC Matrix-EV 256 (*Fig. 11B*), representing the highest accelerated rate of migrated cells after positive control. Furthermore, a lower comparative magnitude was consistent between the RO cohorts, where treatment with RO Stress Matrix-EVs, yielding average counts of 299 and 223 migrated cells, respectively. (*Fig. 11C*)

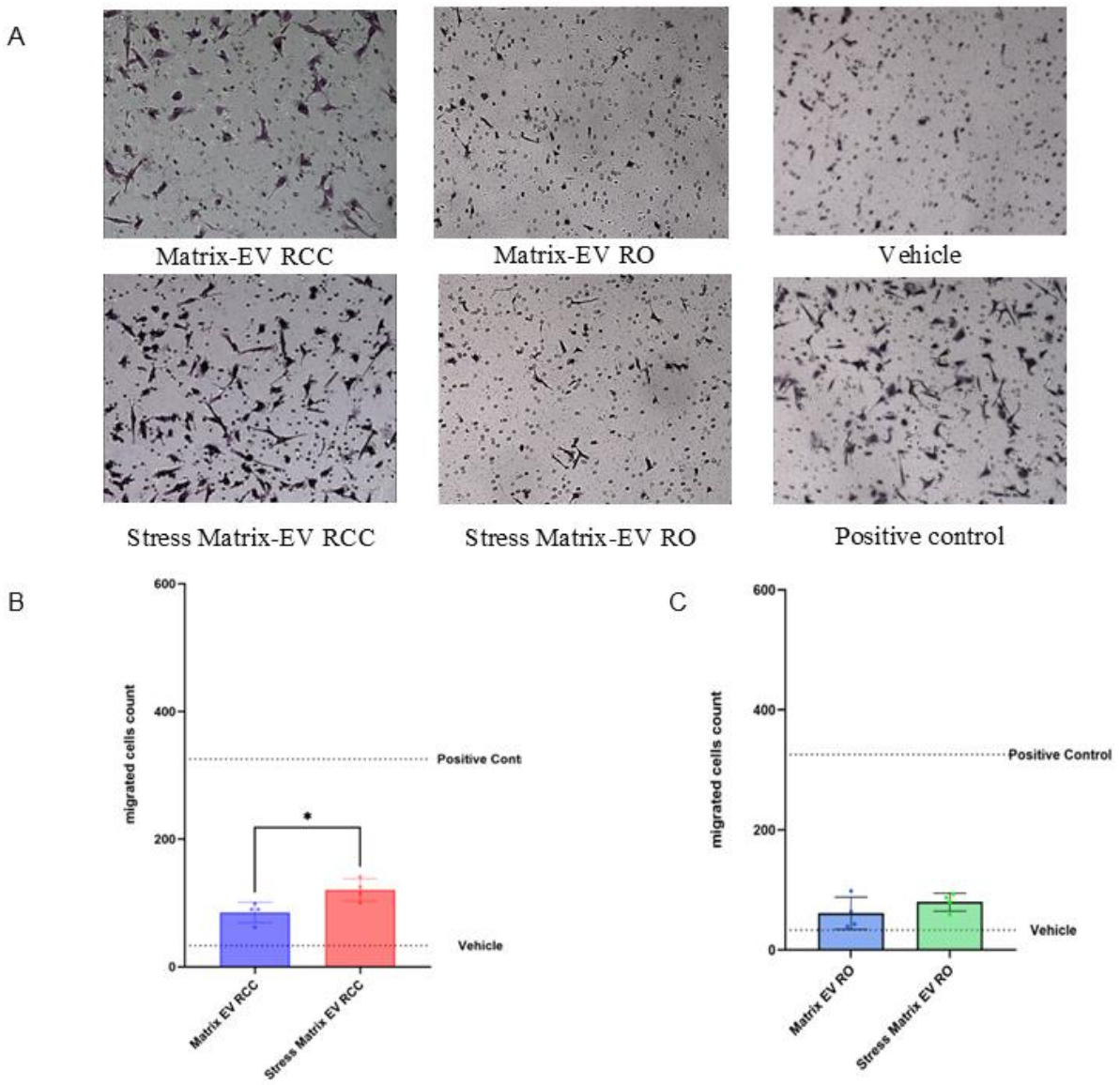

Figure 10. Bar graph comparing the migration of HK-2 cells under Matrix-EV versus Stress Matrix-EV condition.

(A)Leica time-laps images of migrated HK-2 cells following treatment under specified test conditions. (Vehicle, Matrix-EV RCC, Stress Matrix-EV RCC, Matrix-EV RO, Stress Matrix-EV RO, and Positive control). All fields of view are presented at X10 times magnification. (B) Number of migrated HK-2 cells in RCC Matrix-EV versus Stress Matrix-EV conditions. (C) Number of migrated HK-2 cells in RO Matrix-EV versus Stress Matrix-EV conditions. Statistical analysis was performed using an unpaired t-test. (n = 2 EV pools). Data are presented as mean ± SEM; *p<0.05

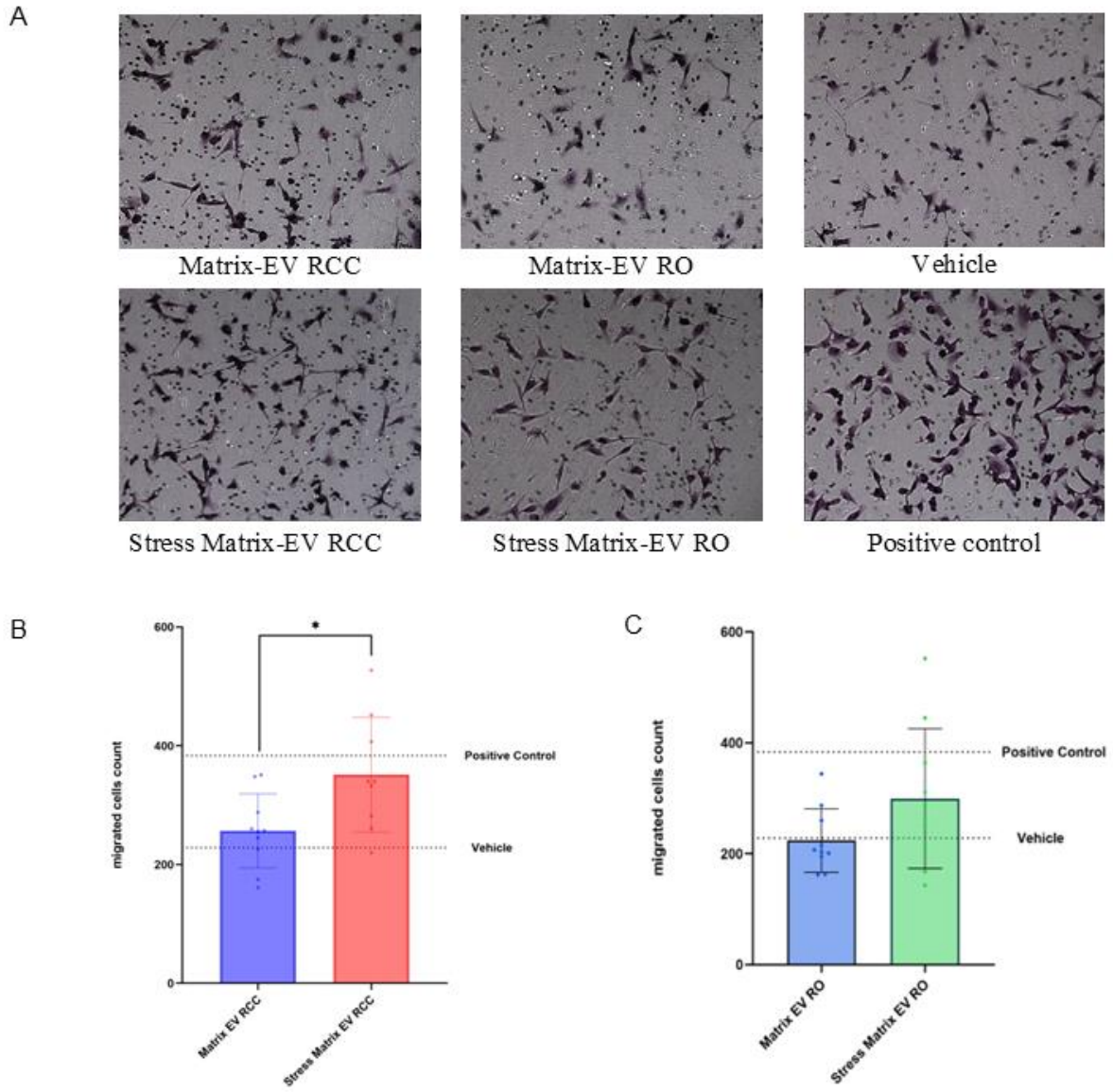

Figure 11. Comparison of 786-O cell migration between Matrix-EV and Stress Matrix-EV conditions.

(A) Leica time-laps images of migrated 786-O cells following treatment under specified test conditions. (Vehicle, Matrix-EV RCC, Stress Matrix-EV RCC, Matrix-EV RO, Stress Matrix-EV RO, and Positive control). All fields of view are presented at X10 times magnification. (B) Number of migrated 786-O cells in RCC Matrix-EV versus Stress Matrix-EV conditions. (C) Number of migrated 786-O cells in RO Matrix-EV versus Stress Matrix-EV conditions. Statistical analysis was performed using an unpaired t-test. (n=2 EV pools). Data are presented as mean ± SEM; *p<0.05

6. Stress Matrix-EVs promote angiogenesis on HMEC-1 cells over 24 hours compared with Matrix-EVs.

To further determine the impact of the mechanically induced EVs on tumor vascularization, angiogenesis assay was performed on the HMEC-1 (Human Microvascular Endothelial) cell line. The angiogenic capacity of the endothelial cells was quantitatively assessed after 24h by measuring three distinct parameters: including total segments length, the number of segments, and the number of mesh structures.

The application of RCC Stress Matrix-EVs generated a statistically significant difference only in number of segments compared to RCC Matrix-EV (122 vs 97) No significant differences were observed in total segment length, number of meshes. In contrast, treatment with RO Stress Matrix-EVs did not alter the total segment length and the total number of segments compared to the RO Matrix-EV control, but was associated with significant increase in the number of meshes, rising from 8.3 meshes in the Matrix-EV group to 17.6 meshes in the Stress Matrix-EV group (*Fig. 12*).

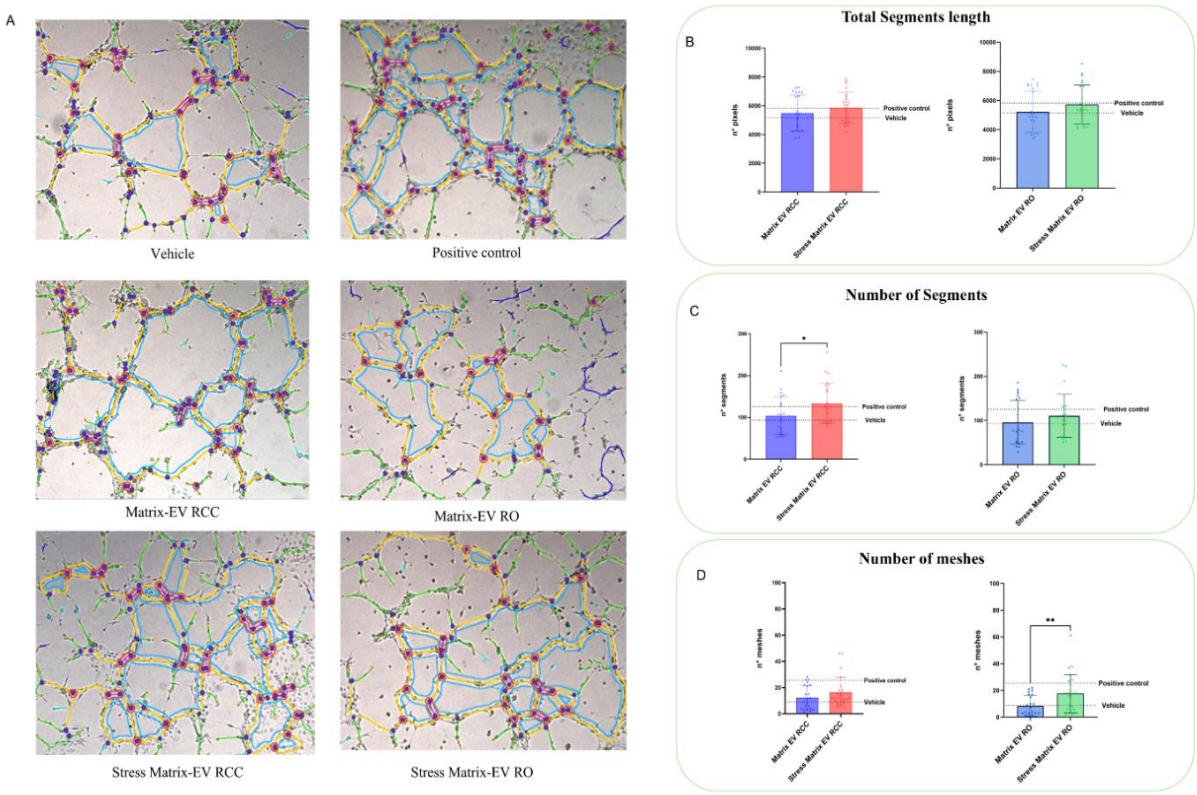

Figure 12. Angiogenic parameters comparison in HMEC-1 cells after treatment with Matrix-EV and Stress Matrix- EVs

(A)Microscopic images of HMEC-1 cells angiogenesis following treatment under specified test conditions. (Vehicle, Matrix-EV RCC, Stress Matrix-EV RCC, Matrix-EV RO, Stress Matrix-EV RO, and Positive control). The images obtained by leica time-laps microscopy were processed and analyzed using the Angiogenesis Analyzer plugin in Fiji (ImageJ). The junctions of the network are red, the functional segments are green and yellow, mesh structures are light blue, and the Isolated or incomplete elements are dark blue color. All fields of view are shown at X10 times magnification. Quantitative analysis of (B) total segment length, (C) total number of segments, and (D) number of closed vascular meshes. In the bar graphs, left panels display values for the RCC models (purple/red) and right panels display values for the RO models (blue/green). Statistical analysis was performed using Mann-Whitney test. (n = 2 EV pools). Data are presented as mean ± SEM]; *p<0.05

Discussion & Conclusion

The present study advances our understanding of the impact of mechanical stress on extracellular vesicle (EV) modulation in renal cell carcinoma (RCC). Pathologically, RCC resides within a biomechanically active environment characterized by solid stresses, matrix stiffness, abnormal blood perfusion and altered interstitial flow (102)Through mechano-transduction, cancer cells convert mechanical inputs into intracellular biochemical signals such as the YAP/TAZ pathway that actively promote metabolic reprogramming, that further leads to cancer stem cells sustainability, and orchestrate pro-metastatic behavior (103–105). Concurrently, recent studies have highlighted EVs as critical messengers that transfer these signals to recipient cells via intercellular communication (106). This research has focused on building a bridge between the two fields, exploring the EV-mediated response of tissue-resident population to mechanical stressors.

Our initial morphological characterization through TEM imaging confirmed that the shape of EVs remained intact across both the isolation processes of matrix-derived and mechanically stimulated extraction. The isolated particles demonstrated the rounded shape and size typical of extracellular vesicles. Additionally, NTA demonstrated a consistent, overlapping size distribution between the two techniques; however, mechanical stimulation resulted in a significantly higher concentration of isolated EVs compared to matrix-based extraction. This observation aligns with recent findings on pancreatic cancer models which demonstrated that the increased matrix stiffness and mechanical rigidity induce the secretion of exosomes by cancer-associated fibroblasts (CAF) (107).

Importantly, while in the same study conducted by Xiao et al., they demonstrated that matrix stiffness increases the total secretion of exosomes, they specifically noted that the effect of the extracellular matrix on the specific molecular contents and surface profiles of these vesicles remains unknown (107). In our study we have addressed this gap through surface profiling of Matrix-EVs and Stress-Matrix EVs via flow cytometry and single-vesicle Leprechaun analysis. This evaluation confirmed the stable and consistent expression of classical tetraspanins (CD9, CD63, CD81) across both groups. In particular, the Leprechaun platform confirmed that this

profiling was structurally conserved, revealing identical marker colocalization patterns with no significant changes in the single, double or triple-positive vesicle subpopulations under mechanical stress. However, further evaluation of a broader marker analysis, revealed specific tumor-associated changes. RCC-derived EVs showed a remarkable shift in their surface landscape upon mechanical stress. This consisted in a strong enrichment of tumor-associated inflammatory signals (MCSP, ROR1), immune-related surface molecules (namely CD8, CD11c, CD86, CD69) and endothelial-surface (CD105, CD146) which was consistent with a reduction in epithelial markers (CD326). These vesicular signatures directly reflect tissue-level pathological features that are known to be the characteristic of malignant renal microenvironment in which tumor samples exhibit a loss of epithelial polarity, immune infiltration, and rapid tissue remodeling (108,109).

In parallel, surface profiling of benign renal oncocytoma-derived Stress Matrix-EVs was characterized by a completely different expression pattern, with no stress-induced accumulation of immune-related surface molecules, nor inflammatory or endothelial markers. However, Stress Matrix-EVs in both malignant and benign cohorts exhibited a significant decrease in the CD326 epithelial marker compared to their corresponding Matrix-EVs, indicating that this alteration might be related to a more general effect of mechanical stress on kidney tissues. Ultimately, this distinct surface profile between RCC- and RO-derived EVs upon mechanical stress underscores the unique capacity of cell populations residing within malignant tissues to respond to physical stimuli, by modulating vesicle release.

Recent research has highlighted an increased release of EVs in response to fluid shear stress (110), however a critical gap remains in our understanding of how these EV produced as a consequence of the physical cues affect the tumor behavior and how they act as mediators of the biomechanical signals.

At a functional level, we have evaluated the effect of Matrix- and Stress Matrix-EVs exposure on normal and tumor cell behaviors such as migration and angiogenesis. For migration, cells were first tested in wound healing assays, which showed that RCC Stress Matrix-EVs accelerated wound closure in HK-2 and 786-O cells compared to the effect exerted by RCC Matrix-EVs. On the other hand, the two cell lines exposed to RO Stress Matrix- and Matrix-EVs did not show any difference in the closure of the created scratch. When HK-2 and 786-O cell lines were tested for migration with a transwell migration assay, we observed the same pattern, with RCC Stress Matrix-

EVs causing a higher rate of migrating cells compared to RCC Matrix-EVs, and no corresponding effect in the RO-derived samples. Together, these findings suggest the ability of EVs that produced under mechanical stress to enhance more aggressive cancer behaviors. Furthermore, this effect was found to be intrinsically dependent on the malignant nature of the tissue of origin, as no differences in migration was observed when cells were exposed to Stress Matrix-EVs from RO tissues compared to their matrix counterpart. This finding is in agreement with recent research demonstrating that mechanical stress in malignant cells leads to pro-tumorigenic alterations in EV surface molecular markers. Indeed, mechanical stress was shown to induces surface enrichment of adhesion molecules and integrins, such as αV and β5, on EVs from breast cancer cells, with a direct effect on recipient cell motility, invasion and organotropic metastasis (111).

The increase in migration observed in HK-2 and 786-O suggests the activation of pathways commonly associated with cancer progression when cells are exposed to RCC Stress Matrix-EVs. Many of the molecular mediators that promote tumor cell motility also contribute to angiogenesis, a process essential for sustaining tumor growth and facilitating metastatic spread (112). Furthermore, mechanical stressors such as tissue stretching and shear stress have been known to regulate angiogenesis via VEGF-related pathways (113,114).

On this basis, we investigated whether the EVs released under mechanical stress conditions might also induce changes in angiogenic activity. We thus tested the response of HMEC-1 endothelial cells to the presence of RCC and RO Matrix- and Stress Matrix-EVs in a tube formation assay.

The exposure to RCC Stress Matrix-EVs resulted in a significant increase in the number of segments, a parameter reflecting the number of individual tubular structures composing the vascular network and often used as an indicator of endothelial branching activity. However, no differences were observed in either the number of meshes, representing the enclosed areas formed by interconnected tubes and associated with maturation and complexity of the network, or the total segment length, which reflects the overall extent of network formation. Therefore, the observed pattern suggests that RCC EVs produced under stress conditions stimulated endothelial remodeling and branching activity without promoting network maturation. Such a phenotype may be indicative of an aberrant angiogenic response, characterized by the formation of numerous but poorly organized vascular structures, a feature frequently observed in the tumor microenvironment (115).

However, additional investigations would be required to determine whether these morphological changes translate into functionally abnormal vessel formation.

In contrast, treatment with RO Stress Matrix-EVs derived from the benign condition resulted in a distinct angiogenic pattern. While the total number of segments and the overall tube length remained unchanged, the number of vascular meshes was significantly increased, approximately doubling compared to control conditions. These findings suggest that, rather than enhancing early sprouting or increasing overall network expansion, Stress Matrix-EVs from benign tissues primarily promote the maturation and interconnection of endothelial structures. The overall rise in angiogenic activity in response to vesicles derived in conditions of mechanical stress regardless of the biological nature of the tissue is consistent with the findings from Wan et al., who showed an increase in angiogenesis from HUVEC when stimulated with stress-derived exosomes from *in vitro* cultured fibroblasts (116). We further showed that endothelial cells exposed to RO Stress Matrix-EVs follow a more physiologically organized angiogenic response compared to the dysregulated pattern observed under RCC-derived or mechanically stressed conditions.

In conclusion, our findings demonstrate that EVs are important mediators of mechanical stress in the kidney tumor microenvironment. Specifically, this mechanical stress affects the TME dynamics by specifically enhancing vesicle release from inflammatory, immunological and endothelial cell populations in malignant tissues but not in benign tissues.

In the context of the present medical literature, our study bridges the knowledge gap regarding the role of EVs in mediating tissue responses to mechanical stressors. We showed that EVs are active mediators of these responses and that they can deliver molecules to other healthy or tumor cells to modify their behavior and promote a malignant phenotype. Crucially, the entire mechanical process is highly dependent on whether the tissue of origin is malignant or benign. Furthermore, we reported that while malignant cells transduce mechanical stress into EVs that promote cell migration and immature angiogenesis and vessel segmentation, benign cells take advantage of these same physical cues to induce functional, and structurally mature vascular networks, without affecting the migratory behavior of healthy and tumor cell lines. However, our study on *in vitro* models lacks the characteristics of a complex physical environment. In future work, *ex vivo* human tissue models, such as organ-on-a-chip and organoids, should be used to more accurately resemble

living systems. Moreover, the lack of cargo characterization poses a great limit in determining the precise pathways that RCC and RO Stess Matrix- and Matrix-EVs modulate within the target cells.

Finally, clarifying of the role of EVs in mechanical stress opens to new promising therapeutic opportunities to target mechanical stress-mediated tumor progression. Notably, we demonstrated that EVs released from malignant and benign tissues under stress exert distinct effects on recipient cells. This divergence suggests the potential to develop targeted therapies that selectively inhibit the malignant EV signalling pathways while preserving normal, non-pathological EV communication

Acknowledgment

I would like to express my sincere gratitude to Professor Federica Collino and Dr. Gaia Bianchi for their guidance, support, and encouragement throughout this research project. I am grateful for their scientific expertise, valuable feedback, and mentoring, which have been indispensable in the completion of this thesis and my academic and professional development. I am truly grateful for the opportunity to work under their supervision at the Nephro-Urology Laboratory.

I would also like to thank all the members of the laboratory for creating a welcoming and collaborative environment. Their kindness, willingness to share their knowledge, and support throughout my internship made this experience both enjoyable and enriching.

I am grateful to my family in Iran for their continuous support and encouragement throughout my studies. Despite the distance, their confidence in me has always been a source of motivation.

I would also like to thank my dear friends Shadi, Sahand, Golnar, Rezaie, Roya, and Ali for their constant encouragement, understanding, and support throughout this journey. Being far from home, they became like a second family to me, providing comfort, companionship, and countless moments of joy during these years. Their friendship and presence have made this experience more meaningful and memorable, and I am truly grateful to have shared this chapter of my life with them.

Finally, I would like to thank my partner, Arian, for his support, patience and encouragement on this journey. I am so grateful to have him with me at this important period in my life.

To everyone who has contributed to my academic journey, directly or indirectly, I extend my sincere gratitude.

BIBLIOGRAPHY

1. Garza FA, Leslie SW. Anatomy, Abdomen and Pelvis: Kidneys. In. StatPearls Publishing; 2025.

2. Luyckx VA., Chertow GM., Yu ASL., Marsden PA., Skorecki Karl, Taal MW. Brenner & Rector's the kidney. 12th Edition. Elsevier Health Sciences; 2026. 2404 p.

3. Harper S, Unwin R, Firth JD. Structure and function of the kidney. In: Oxford Textbook of Medicine. Oxford University PressOxford; 2020. p. 4717–28. doi:10.1093/med/9780198746690.003.0472update_001

4. Kam P, Power I, Cousins MJ, Siddal PJ. Functions of the Kidneys and Functional Anatomy. In: Principles of Physiology for the Anaesthetist. 4th Edition. CRC Press; 2020.

5. Zhuo JL, Li XC. Proximal Nephron. In: Comprehensive Physiology. Wiley; 2013. p. 1079– doi:10.1002/cphy.c110061

6. Mount DB. Thick ascending limb of the loop of Henle. Clin J Am Soc Nephrol. 2014 Nov 7;9(11):1974–86. doi:10.2215/CJN.04480413 PubMed PMID: 25318757.

7. Cheng L, Poulsen SB, Wu Q, Esteva-Font C, Olesen ETB, Peng L, et al. Rapid Aldosterone-Mediated Signaling in the DCT Increases Activity of the Thiazide-Sensitive NaCl Cotransporter. Journal of the American Society of Nephrology. 2019 Aug;30(8):1454–70. doi:10.1681/ASN.2018101025

8. Suchy-Dicey AM, Laha T, Hoofnagle A, Newitt R, Sirich TL, Meyer TW, et al. Tubular Secretion in CKD. J Am Soc Nephrol. 2016 Jul;27(7):2148–55. doi:10.1681/ASN.2014121193 PubMed PMID: 26614381.

9. Carroll, Robert G. Elsevier's Integrated Physiology. Elsevier; 2006.

10. Fontecha-Barriuso M, Lopez-Diaz AM, Guerrero-Mauvecin J, Miguel V, Ramos AM, Sanchez-Niño MD, et al. Tubular Mitochondrial Dysfunction, Oxidative Stress, and Progression of Chronic Kidney Disease. Antioxidants (Basel). 2022 Jul 12;11(7). doi:10.3390/antiox11071356 PubMed PMID: 35883847.

11. Qin Z, Xu Q, Hu H, Yu L, Zeng S. Extracellular Vesicles in Renal Cell Carcinoma: Multifaceted Roles and Potential Applications Identified by Experimental and Computational Methods. Front Oncol. 2020;10:724. doi:10.3389/fonc.2020.00724 PubMed PMID: 32457844.

12. Adhipandito CF, Cheung SH, Lin YH, Wu SH. Atypical Renal Clearance of Nanoparticles Larger Than the Kidney Filtration Threshold. Int J Mol Sci. 2021 Oct 17;22(20). doi:10.3390/ijms222011182 PubMed PMID: 34681853.

13. Thorstenson A, Bergman M, Scherman-Plogell AH, Hosseinnia S, Ljungberg B, Adolfsson J, et al. Tumour characteristics and surgical treatment of renal cell carcinoma in Sweden 2005-2010: a population-based study from the national Swedish kidney cancer register. Scand J Urol. 2014 Jun;48(3):231–8. doi:10.3109/21681805.2013.864698 PubMed PMID: 24666102.

14. Bray F, Laversanne M, Sung H, Ferlay J, Siegel RL, Soerjomataram I, et al. Global cancer statistics 2022: GLOBOCAN estimates of incidence and mortality worldwide for 36 cancers in 185 countries. CA Cancer J Clin. 2024;74(3):229–63. doi:10.3322/caac.21834 PubMed PMID: 38572751.

15. Rinaldi L, Senatore E, Feliciello S, Chiuso F, Insabato L, Feliciello A. Kidney cancer: From tumor biology to innovative therapeutics. Biochim Biophys Acta Rev Cancer. 2025 Feb;1880(1):189240. doi:10.1016/j.bbcan.v2024.189240 PubMed PMID: 39674419.

16. Capitanio U, Bensalah K, Bex A, Boorjian SA, Bray F, Coleman J, et al. Epidemiology of Renal Cell Carcinoma. Eur Urol. 2019 Jan;75(1):74–84. doi:10.1016/j.eururo.2018.08.036 PubMed PMID: 30243799.

17. Rosen RD, Sapra A. TNM Classification. 2026. PubMed PMID: 31985980.

18. Moch H. [The WHO/ISUP grading system for renal carcinoma]. Pathologe. 2016 Jul;37(4):355–60. doi:10.1007/s00292-016-0171-y PubMed PMID: 27271258.

19. Bex A, Ghanem YA, Albiges L, Bonn S, Campi R, Capitanio U, et al. European Association of Urology Guidelines on Renal Cell Carcinoma: The 2025 Update. Eur Urol. 2025 Jun;87(6):683–96. doi:10.1016/j.eururo.2025.02.020 PubMed PMID: 40118739.

20. Tahbaz R, Schmid M, Merseburger AS. Prevention of kidney cancer incidence and recurrence: lifestyle, medication and nutrition. Curr Opin Urol. 2018 Jan;28(1):62–79. doi:10.1097/MOU.0000000000000454 PubMed PMID: 29059103.

21. Moradi A, Fann J, Zhang G, Pal SK, Sadimin E. Beyond clear cell: Rare histologic and molecular variants of renal cell carcinoma. Urologic Oncology: Seminars and Original Investigations. 2026 Mar;111066. doi:10.1016/j.urolonc.2026.111066

22. Gómez-Virgilio L, Velazquez-Paniagua M, Cuazozon-Ferrer L, Silva-Lucero MDC, Gutierrez-Malacara AI, Padilla-Mendoza JR, et al. Genetics, Pathophysiology, and Current Challenges in Von Hippel-Lindau Disease Therapeutics. Diagnostics (Basel). 2024 Aug 29;14(17). doi:10.3390/diagnostics14171909 PubMed PMID: 39272694.

23. Mazumder S, Higgins PJ, Samarakoon R. Downstream Targets of VHL/HIF-α Signaling in Renal Clear Cell Carcinoma Progression: Mechanisms and Therapeutic Relevance. Cancers (Basel). 2023 Feb 19;15(4). doi:10.3390/cancers15041316 PubMed PMID: 36831657.

24. Krieg M, Haas R, Brauch H, Acker T, Flamme I, Plate KH. Up-regulation of hypoxia-inducible factors HIF-1alpha and HIF-2alpha under normoxic conditions in renal carcinoma cells by von Hippel-Lindau tumor suppressor gene loss of function. Oncogene. 2000 Nov 16;19(48):5435–43. doi:10.1038/sj.onc.1203938 PubMed PMID: 11114720.

25. Courthod G, Tucci M, Di Maio M, Scagliotti G V. Papillary renal cell carcinoma: A review of the current therapeutic landscape. Crit Rev Oncol Hematol. 2015 Oct;96(1):100–12. doi:10.1016/j.critrevonc.2015.05.008 PubMed PMID: 26052049.

26. Bahadoram S, Davoodi M, Hassanzadeh S, Bahadoram M, Barahman M, Mafakher L. Renal cell carcinoma: an overview of the epidemiology, diagnosis, and treatment. G Ital Nefrol. 2022 Jun 20;39(3). PubMed PMID: 35819037.

27. Yanus GA, Kuligina ES, Imyanitov EN. Hereditary Renal Cancer Syndromes. Med Sci (Basel). 2024 Feb 18;12(1). doi:10.3390/medsci12010012 PubMed PMID: 38390862.

28. Filippiadis D, Mauri G, Marra P, Charalampopoulos G, Gennaro N, De Cobelli F. Percutaneous ablation techniques for renal cell carcinoma: current status and future trends. Int J Hyperthermia. 2019 Oct;36(2):21–30. doi:10.1080/02656736.2019.1647352 PubMed PMID: 31537160.

29. Di Marco F, Pani A, Floris M, Martini A, Dell'Antonio G, Capitanio U, et al. Unexpected Outcomes of Renal Function after Radical Nephrectomy: Histology Relevance along with Clinical Aspects. J Clin Med. 2021 Jul 28;10(15). doi:10.3390/jcm10153322 PubMed PMID: 34362105.

30. Gaffen SL, Liu KD. Overview of interleukin-2 function, production and clinical applications. Cytokine. 2004 Nov 7;28(3):109–23. doi:10.1016/j.cyto.2004.06.010 PubMed PMID: 15473953.

31. Yang J, Wang K, Yang Z. Treatment strategies for clear cell renal cell carcinoma: Past, present and future. Front Oncol. 2023;13:1133832. doi:10.3389/fonc.2023.1133832 PubMed PMID: 37025584.

32. Gossage L, Eisen T, Maher ER. VHL, the story of a tumour suppressor gene. Nat Rev Cancer. 2015 Jan;15(1):55–64. doi:10.1038/nrc3844 PubMed PMID: 25533676.

33. Pal K, Madamsetty VS, Dutta SK, Wang E, Angom RS, Mukhopadhyay D. Synchronous inhibition of mTOR and VEGF/NRP1 axis impedes tumor growth and metastasis in renal cancer. NPJ Precis Oncol. 2019;3:31. doi:10.1038/s41698-019-0105-2 PubMed PMID: 31840081.

34. Atkins MB, Tannir NM. Current and emerging therapies for first-line treatment of metastatic clear cell renal cell carcinoma. Cancer Treat Rev. 2018 Nov;70:127–37. doi:10.1016/j.ctrv.2018.07.009 PubMed PMID: 30173085.

35. Escudier B, Szczylik C, Hutson TE, Demkow T, Staehler M, Rolland F, et al. Randomized phase II trial of first-line treatment with sorafenib versus interferon Alfa-2a in patients with metastatic renal cell carcinoma. J Clin Oncol. 2009 Mar 10;27(8):1280–9. cdoi:10.1200/JCO.2008.19.3342 PubMed PMID: 19171708.

36. Motzer RJ, Hutson TE, Tomczak P, Michaelson MD, Bukowski RM, Rixe O, et al. Sunitinib versus interferon alfa in metastatic renal-cell carcinoma. N Engl J Med. 2007 Jan 11;356(2):115–24. doi:10.1056/NEJMoa065044 PubMed PMID: 17215529.

37. Comandone A, Vana F, Comandone T, Tucci M. Antiangiogenic Therapy in Clear Cell Renal Carcinoma (CCRC): Pharmacological Basis and Clinical Results. Cancers (Basel). 2021 Nov 24;13(23). doi:10.3390/cancers13235896 PubMed PMID: 34885006.

38. Andrews LP, Yano H, Vignali DAA. Inhibitory receptors and ligands beyond PD-1, PD-L1 and CTLA-4: breakthroughs or backups. Nat Immunol. 2019 Nov;20(11):1425–34. doi:10.1038/s41590-019-0512-0 PubMed PMID: 31611702.

39. Rini BI, Plimack ER, Stus V, Gafanov R, Hawkins R, Nosov D, et al. Pembrolizumab plus Axitinib versus Sunitinib for Advanced Renal-Cell Carcinoma. N Engl J Med. 2019 Mar 21;380(12):1116–27. doi:10.1056/NEJMoa1816714 PubMed PMID: 30779529.

40. Motzer R, Alekseev B, Rha SY, Porta C, Eto M, Powles T, et al. Lenvatinib plus Pembrolizumab or Everolimus for Advanced Renal Cell Carcinoma. N Engl J Med. 2021 Apr 8;384(14):1289–300. doi:10.1056/NEJMoa2035716 PubMed PMID: 33616314.

41. Choueiri TK, Powles T, Burotto M, Escudier B, Bourlon MT, Zurawski B, et al. Nivolumab plus Cabozantinib versus Sunitinib for Advanced Renal-Cell Carcinoma. N Engl J Med. 2021 Mar 4;384(9):829–41. doi:10.1056/NEJMoa2026982 PubMed PMID: 33657295.

42. Motzer RJ, Hutson TE, Glen H, Michaelson MD, Molina A, Eisen T, et al. Lenvatinib, everolimus, and the combination in patients with metastatic renal cell carcinoma: a randomised, phase 2, open-label, multicentre trial. Lancet Oncol. 2015 Nov;16(15):1473–82. doi:10.1016/S1470-2045(15)00290-9 PubMed PMID: 26482279.

43. Motzer RJ, Hutson TE, Ren M, Dutcus C, Larkin J. Independent assessment of lenvatinib plus everolimus in patients with metastatic renal cell carcinoma. Lancet Oncol. 2016 Jan;17(1):e4-5. doi:10.1016/S1470-2045(15)00543-4 PubMed PMID: 26758760.

44. Lu Y, Zhang M, Zhou J, Liu X, Wang L, Hu X, et al. Extracellular vesicles in renal cell carcinoma: challenges and opportunities coexist. Front Immunol. 2023;14:1212101. doi:10.3389/fimmu.2023.1212101 PMID: 37469514.

45. Welsh JA, Goberdhan DCI, O'Driscoll L, Buzas EI, Blenkiron C, Bussolati B, et al. Minimal information for studies of extracellular vesicles (MISEV2023): From basic to advanced approaches. J Extracell Vesicles. 2024 Feb;13(2):e12404. doi:10.1002/jev2.12404 PubMed PMID: 38326288.

46. Lee YJ, Shin KJ, Chae YC. Regulation of cargo selection in exosome biogenesis and its biomedical applications in cancer. Exp Mol Med. 2024 Apr;56(4):877–89. doi:10.1038/s12276-024-01209-y PubMed PMID: 38580812.

47. Crescitelli R, Lässer C, Lötvall J. Isolation and characterization of extracellular vesicle subpopulations from tissues. Nat Protoc. 2021 Mar;16(3):1548–80. doi:10.1038/s41596-020-00466-1%20 PubMed PMID: 33495626.

48. Henne WM, Stenmark H, Emr SD. Molecular mechanisms of the membrane sculpting ESCRT pathway. Cold Spring Harb Perspect Biol. 2013 Sep 1;5(9). doi:10.1101/cshperspect.a016766 PubMed PMID: 24003212.

49. Henne WM, Buchkovich NJ, Emr SD. The ESCRT pathway. Dev Cell. 2011 Jul 19;21(1):77–91. doi:10.1016/j.devcel.2011.05.015 PubMed PMID: 21763610.

50. Han QF, Li WJ, Hu KS, Gao J, Zhai WL, Yang JH, et al. Exosome biogenesis: machinery, regulation, and therapeutic implications in cancer. Mol Cancer. 2022 Nov 1;21(1):207. doi:10.1186/s12943-022-01671-0 PMID: 36320056.

51. van Niel G, Porto-Carreiro I, Simoes S, Raposo G. Exosomes: a common pathway for a specialized function. J Biochem. 2006 Jul;140(1):13–21. doi:10.1093/jb/mvj128 PubMed PMID: 16877764.

52. Hugel B, Martínez MC, Kunzelmann C, Freyssinet JM. Membrane microparticles: two sides of the coin. Physiology (Bethesda). 2005 Feb;20:22–7. doi:10.1152/physiol.00029.2004 PubMed PMID: 15653836.

53. Akers JC, Gonda D, Kim R, Carter BS, Chen CC. Biogenesis of extracellular vesicles (EV): exosomes, microvesicles, retrovirus-like vesicles, and apoptotic bodies. J Neurooncol. 2013 May;113(1):1–11. doi:10.1007/s11060-013-1084-8 PubMed PMID: 23456661.

54. Muralidharan-Chari V, Clancy J, Plou C, Romao M, Chavrier P, Raposo G, et al. ARF6-regulated shedding of tumor cell-derived plasma membrane microvesicles. Curr Biol. 2009 Dec 1;19(22):1875–85. doi:10.1016/j.cub.2009.09.059 PubMed PMID: 19896381.

55. Mori T, Giovannelli L, Bilia AR, Margheri F. Exosomes: Potential Next-Generation Nanocarriers for the Therapy of Inflammatory Diseases. Pharmaceutics. 2023 Sep 4;15(9). doi:10.3390/pharmaceutics15092276 PubMed PMID: 37765245.

56. Schank MB, Zhao J, Wang L, Moorman JP, Yao ZQ. Extracellular Vesicles: A Comprehensive Review of Their Origins, Functions, and Therapeutic Potential. Biomedicines. 2026 Feb 25;14(3). doi:10.3390/biomedicines14030495 PubMed PMID: 41898142.

57. Becker A, Thakur BK, Weiss JM, Kim HS, Peinado H, Lyden D. Extracellular Vesicles in Cancer: Cell-to-Cell Mediators of Metastasis. Cancer Cell. 2016 Dec 12;30(6):836–48. doi:10.1016/j.ccell.2016.10.009 PubMed PMID: 27960084.

58. Jang SC, Crescitelli R, Cvjetkovic A, Belgrano V, Olofsson Bagge R, Sundfeldt K, et al. Mitochondrial protein enriched extracellular vesicles discovered in human melanoma tissues can be detected in patient plasma. J Extracell Vesicles. 2019;8(1):1635420. doi:10.1080/20013078.2019.1635420 PubMed PMID: 31497264.

59. Mincheva-Nilsson L, Baranov V, Nagaeva O, Dehlin E. Isolation and Characterization of Exosomes from Cultures of Tissue Explants and Cell Lines. Curr Protoc Immunol. 2016 Nov 1;115:14.42.1-14.42.21. doi:10.1002/cpim.17 PubMed PMID: 27801511.

60. Vella LJ, Scicluna BJ, Cheng L, Bawden EG, Masters CL, Ang CS, et al. A rigorous method to enrich for exosomes from brain tissue. J Extracell Vesicles. 2017;6(1):1348885. doi:10.1080/20013078.2017.1348885 PubMed PMID: 28804598.

61. Crescitelli R, Lässer C, Jang SC, Cvjetkovic A, Malmhäll C, Karimi N, et al. Subpopulations of extracellular vesicles from human metastatic melanoma tissue identified by quantitative proteomics after optimized isolation. J Extracell Vesicles. 2020;9(1):1722433. doi:10.1080/20013078.2020.1722433 PubMed PMID: 32128073.

62. Zhi Z, Sun Q, Tang W. Research advances and challenges in tissue-derived extracellular vesicles. Front Mol Biosci. 2022;9:1036746. doi:10.3389/fmolb.2022.1036746 PubMed PMID: 36589228.

63. Dunn GP, Old LJ, Schreiber RD. The immunobiology of cancer immunosurveillance and immunoediting. Immunity. 2004 Aug;21(2):137–48. doi:10.1016/j.immuni.2004.07.017 PMID: 15308095.

64. Grange C, Tapparo M, Tritta S, Deregibus MC, Battaglia A, Gontero P, et al. Role of HLA-G and extracellular vesicles in renal cancer stem cell-induced inhibition of dendritic cell differentiation. BMC Cancer. 2015 Dec 24;15:1009. doi:10.1186/s12885-015-2025-z PubMed PMID: 26704308.

65. Yang L, Wu X, Wang D, Luo C, Chen L. Renal carcinoma cell-derived exosomes induce human immortalized line of Jurkat T lymphocyte apoptosis in vitro. Urol Int. 2013;91(3):363–9. doi:10.1159/000348747 PubMed PMID: 23921176.

66. Xia Y, Zhang Q, Zhen Q, Zhao Y, Liu N, Li T, et al. Negative regulation of tumor-infiltrating NK cell in clear cell renal cell carcinoma patients through the exosomal pathway. Oncotarget. 2017 Jun 6;8(23):37783–95. doi:10.18632/oncotarget.16354 PubMed PMID: 28384121.

67. Gao Y, Xu H, Li N, Wang H, Ma L, Chen S, et al. Renal cancer-derived exosomes induce tumor immune tolerance by MDSCs-mediated antigen-specific immunosuppression. Cell Commun Signal. 2020 Jul 8;18(1):106. doi:10.1186/s12964-020-00611-z PubMed PMID: 32641056.

68. Diao J, Yang X, Song X, Chen S, He Y, Wang Q, et al. Exosomal Hsp70 mediates immunosuppressive activity of the myeloid-derived suppressor cells via phosphorylation of Stat3. Med Oncol. 2015 Feb;32(2):453. doi:10.1007/s12032-014-0453-2 PubMed PMID: 25603952.

69. Huang X, Wang J, Guan J, Zheng Z, Hao J, Sheng Z, et al. Exosomal Circsafb2 Reshaping Tumor Environment to Promote Renal Cell Carcinoma Progression by Mediating M2 Macrophage Polarization. Front Oncol. 2022;12:808888. doi:10.3389/fonc.2022.808888 PubMed PMID: 35646637.

70. Greenberg JW, Kim H, Ahn M, Moustafa AA, Zhou H, Barata PC, et al. Combination of Tipifarnib and Sunitinib Overcomes Renal Cell Carcinoma Resistance to Tyrosine Kinase Inhibitors via Tumor-Derived Exosome and T Cell Modulation. Cancers (Basel). 2022 Feb 11;14(4). doi:10.3390/cancers14040903 PubMed PMID: 35205655.

71. Che X, Su W, Li X, Liu N, Wang Q, Wu G. Angiogenesis Pathway in Kidney Renal Clear Cell Carcinoma and Its Prognostic Value for Cancer Risk Prediction. Front Med (Lausanne). 2021;8:731214. doi:10.3389/fmed.2021.731214 PubMed PMID: 34778292.

72. Guillaume Z, Auvray M, Vano Y, Oudard S, Helley D, Mauge L. Renal Carcinoma and Angiogenesis: Therapeutic Target and Biomarkers of Response in Current Therapies. Cancers (Basel). 2022 Dec 14;14(24). doi:10.3390/cancers14246167 PubMed PMID: 36551652.

73. Horie K, Kawakami K, Fujita Y, Sugaya M, Kameyama K, Mizutani K, et al. Exosomes expressing carbonic anhydrase 9 promote angiogenesis. Biochem Biophys Res Commun. 2017 Oct 21;492(3):356–61. doi:10.1016/j.bbrc.2017.08.107 PubMed PMID: 28851650.

74. Lindoso RS, Collino F, Camussi G. Extracellular vesicles derived from renal cancer stem cells induce a pro-tumorigenic phenotype in mesenchymal stromal cells. Oncotarget. 2015 Apr 10;6(10):7959–69doi:10.18632/oncotarget.3503 PubMed PMID: 25797265.

75. Grange C, Tapparo M, Collino F, Vitillo L, Damasco C, Deregibus MC, et al. Microvesicles released from human renal cancer stem cells stimulate angiogenesis and formation of lung premetastatic niche. Cancer Res. 2011 Aug 1;71(15):5346–56. doi:10.1158/0008-5472.CAN-11-0241 PubMed PMID: 21670082.

76. López-Soto A, Gonzalez S, Smyth MJ, Galluzzi L. Control of Metastasis by NK Cells. Cancer Cell. 2017 Aug 14;32(2):135–54. doi:10.1016/j.ccell.2017.06.009 PubMed PMID: 28810142.

77. Jin C, Shi L, Li K, Liu W, Qiu Y, Zhao Y, et al. Mechanism of tumor-derived extracellular vesicles in regulating renal cell carcinoma progression by the delivery of MALAT1. Oncol Rep. 2021 Sep;46(3). doi:10.3892/or.2021.8138 PubMed PMID: 34278501.

78. Wang L, Yang G, Zhao D, Wang J, Bai Y, Peng Q, et al. CD103-positive CSC exosome promotes EMT of clear cell renal cell carcinoma: role of remote MiR-19b-3p. Mol Cancer. 2019 Apr 11;18(1):86. doi:10.1186/s12943-019-0997-z PubMed PMID: 30975145.

79. Fu W, Zhao H, Liu Y, Nie H, Gao B, Yin F, et al. Exosomes Derived from Cancer-Associated Fibroblasts Regulate Cell Progression in Clear-Cell Renal-Cell Carcinoma. Nephron. 2022;146(4):383–92. doi:10.1159/000520304 PubMed PMID: 34903693.

80. Jingushi K, Uemura M, Ohnishi N, Nakata W, Fujita K, Naito T, et al. Extracellular vesicles isolated from human renal cell carcinoma tissues disrupt vascular endothelial cell morphology via azurocidin. Int J Cancer. 2018 Feb 1;142(3):607–17. doi:10.1002/ijc.31080 PubMed PMID: 28975613.

81. Xuan Z, Chen C, Tang W, Ye S, Zheng J, Zhao Y, et al. TKI-Resistant Renal Cancer Secretes Low-Level Exosomal miR-549a to Induce Vascular Permeability and Angiogenesis to Promote Tumor Metastasis. Front Cell Dev Biol. 2021;9:689947. doi:10.3389/fcell.2021.689947 PubMed PMID: 34179017.

82. Xavier CPR, Belisario DC, Rebelo R, Assaraf YG, Giovannetti E, Kopecka J, et al. The role of extracellular vesicles in the transfer of drug resistance competences to cancer cells. Drug Resist Updat. 2022 May;62:100833. doi:10.1016/j.drup.2022.100833 PubMed PMID: 35429792.

83. Qu L, Ding J, Chen C, Wu ZJ, Liu B, Gao Y, et al. Exosome-Transmitted lncARSR Promotes Sunitinib Resistance in Renal Cancer by Acting as a Competing Endogenous RNA. Cancer Cell. 2016 May 9;29(5):653–68. doi:10.1016/j.ccell.2016.03.004 PubMed PMID: 27117758.

84. Pan Y, Lu X, Shu G, Cen J, Lu J, Zhou M, et al. Extracellular Vesicle-Mediated Transfer of LncRNA IGFL2-AS1 Confers Sunitinib Resistance in Renal Cell Carcinoma. Cancer Res.

2023 Jan 4;83(1):103–16. doi:10.1158/0008-5472.CAN-21-3432 PubMed PMID: 36264173.

85. Lim AR, Vincent BG, Weaver AM, Rathmell WK. Sunitinib and Axitinib increase secretion and glycolytic activity of small extracellular vesicles in renal cell carcinoma. Cancer Gene Ther. 2022 Jun;29(6):683–96. doi:10.1038/s41417-021-00345-1 PubMed PMID: 34088993.

86. He J, He J, Min L, He Y, Guan H, Wang J, et al. Extracellular vesicles transmitted miR-31-5p promotes sorafenib resistance by targeting MLH1 in renal cell carcinoma. Int J Cancer. 2020 Feb 15;146(4):1052–63. doi:10.1002/ijc.32543 PubMed PMID: 31259424.

87. Vento JA, Rini BI. Treatment of Refractory Metastatic Renal Cell Carcinoma. Cancers (Basel). 2022 Oct 13;14(20). doi:10.3390/cancers14205005 PubMed PMID: 36291789.

88. Kamerkar S, LeBleu VS, Sugimoto H, Yang S, Ruivo CF, Melo SA, et al. Exosomes facilitate therapeutic targeting of oncogenic KRAS in pancreatic cancer. Nature. 2017 Jun 22;546(7659):498–503. doi:10.1038/nature22341v PubMed PMID: 28607485.

89. Cheng L, Hill AF. Therapeutically harnessing extracellular vesicles. Nat Rev Drug Discov. 2022 May;21(5):379–99. doi:10.1038/s41573-022-00410-w PubMed PMID: 35236964.

90. Zhou M, Wang L, Yu B, He J, Zhang J, Liu Z, et al. How Advanced Are Extracellular Vesicles in Renal Cell Carcinoma? For Diagnostic and Therapeutic Frontiers. Int J Nanomedicine. 2025;20:10963–76. doi:10.2147/IJN.S545749 PubMed PMID: 40949610.

91. Wen H, Zheng S, Zhu X, Wang L, Chen D. Characteristics of the tumor microenvironment and potential immunotherapy strategies in renal cell carcinoma. Front Immunol. 2025;16:1643533. doi:10.3389/fimmu.2025.1643533 PubMed PMID: 40963620.

92. Liu Q, Luo Q, Ju Y, Song G. Role of the mechanical microenvironment in cancer development and progression. Cancer Biol Med. 2020 May 15;17(2):282–92. doi:10.20892/j.issn.2095-3941.2019.0437 PubMed PMID: 32587769.

93. Kaelin WG. The von Hippel-Lindau tumor suppressor protein and clear cell renal carcinoma. Clin Cancer Res. 2007 Jan 15;13(2 Pt 2):680s–4s. doi:10.1158/1078-0432.CCR-06-1865 PubMed PMID: 17255293.

94. Liu Q, Luo Q, Ju Y, Song G. Role of the mechanical microenvironment in cancer development and progression. Cancer Biol Med. 2020 May 15;17(2):282–92. doi:10.20892/j.issn.2095-3941.2019.0437 PubMed PMID: 32587769.

95. Przybyla L, Muncie JM, Weaver VM. Mechanical Control of Epithelial-to-Mesenchymal Transitions in Development and Cancer. Annu Rev Cell Dev Biol. 2016 Oct 6;32:527–54. doi:10.1146/annurev-cellbio-111315-125150 PubMed PMID: 27298087.

96. Zanconato F, Cordenonsi M, Piccolo S. YAP/TAZ at the Roots of Cancer. Cancer Cell. 2016 Jun 13;29(6):783–803. doi:10.1016/j.ccell.2016.05.005v PubMed PMID: 27300434.

97. Shuch B, Amin A, Armstrong AJ, Eble JN, Ficarra V, Lopez-Beltran A, et al. Understanding pathologic variants of renal cell carcinoma: distilling therapeutic opportunities from

biologic complexity. Eur Urol. 2015 Jan;67(1):85–97. doi:10.1016/j.eururo.2014.04.029 PubMed PMID: 24857407.

98. Marozzi M, Parnigoni A, Negri A, Viola M, Vigetti D, Passi A, et al. Inflammation, Extracellular Matrix Remodeling, and Proteostasis in Tumor Microenvironment. Int J Mol Sci. 2021 Jul 28;22(15). doi:10.3390/ijms22158102 PubMed PMID: 34360868.

99. Patwardhan S, Mahadik P, Shetty O, Sen S. ECM stiffness-tuned exosomes drive breast cancer motility through thrombospondin-1. Biomaterials. 2021 Dec;279:121185. doi:10.1016/j.biomaterials.2021.121185 PubMed PMID: 34808560.

100. Shuch B, Amin A, Armstrong AJ, Eble JN, Ficarra V, Lopez-Beltran A, et al. Understanding pathologic variants of renal cell carcinoma: distilling therapeutic opportunities from biologic complexity. Eur Urol. 2015 Jan;67(1):85–97. doi:10.1016/j.eururo.2014.04.029 PubMed PMID: 24857407.

101. Shuch B, Amin A, Armstrong AJ, Eble JN, Ficarra V, Lopez-Beltran A, et al. Understanding pathologic variants of renal cell carcinoma: distilling therapeutic opportunities from biologic complexity. Eur Urol. 2015 Jan;67(1):85–97. doi:10.1016/j.eururo.2014.04.029 PubMed PMID: 24857407.

102. Pickup MW, Mouw JK, Weaver VM. The extracellular matrix modulates the hallmarks of cancer. EMBO Rep. 2014 Dec;15(12):1243–53. doi:10.15252/embr.201439246 PubMed PMID: 25381661.

103. Bertero T, Oldham WM, Grasset EM, Bourget I, Boulter E, Pisano S, et al. Tumor-Stroma Mechanics Coordinate Amino Acid Availability to Sustain Tumor Growth and Malignancy. Cell Metab. 2019 Jan 8;29(1):124-140.e10. doi:10.1016/j.cmet.2018.09.012 PubMed PMID: 30293773.

104. Guo L, Cui C, Zhang K, Wang J, Wang Y, Lu Y, et al. Kindlin-2 links mechano-environment to proline synthesis and tumor growth. Nat Commun. 2019 Feb 19;10(1):845. doi:10.1038/s41467-019-08772-3 PubMed PMID: 30783087.

105. Broders-Bondon F, Nguyen Ho-Bouldoires TH, Fernandez-Sanchez ME, Farge E. Mechanotransduction in tumor progression: The dark side of the force. J Cell Biol. 2018 May 7;217(5):1571–87. doi:10.1083/jcb.201701039 PubMed PMID: 29467174.

106. Raposo G, Stoorvogel W. Extracellular vesicles: exosomes, microvesicles, and friends. J Cell Biol. 2013 Feb 18;200(4):373–83. doi:10.1083/jcb.201211138 PubMed PMID: 23420871.

107. Xiao W, Pahlavanneshan M, Eun CY, Zhang X, DeKalb C, Mahgoub B, et al. Matrix stiffness mediates pancreatic cancer chemoresistance through induction of exosome hypersecretion in a cancer associated fibroblasts-tumor organoid biomimetic model. Matrix Biol Plus. 2022 Jun;14:100111. doi:10.1016/j.mbplus.2022.100111 PubMed PMID: 35619988.

108. Gargalionis AN, Papavassiliou KA, Papavassiliou AG. Mechanobiology of solid tumors. Biochim Biophys Acta Mol Basis Dis. 2022 Dec 1;1868(12):166555. doi:10.1016/j.bbadis.2022.166555 PubMed PMID: 36150659.

109. Giraldo NA, Becht E, Pagès F, Skliris G, Verkarre V, Vano Y, et al. Orchestration and Prognostic Significance of Immune Checkpoints in the Microenvironment of Primary and Metastatic Renal Cell Cancer. Clin Cancer Res. 2015 Jul 1;21(13):3031–40. doi:10.1158/1078-0432.CCR-14-2926 PubMed PMID: 25688160.

110. Sangha GS, Weber CM, Sapp RM, Setua S, Thangaraju K, Pettebone M, et al. Mechanical stimuli such as shear stress and piezo1 stimulation generate red blood cell extracellular vesicles. Front Physiol. 2023;14:1246910 doi:10.3389/fphys.2023.1246910 PubMed PMID: 37719461.

111. Saquel C, Bochler L, MacDonald E, Gracia C, Viaris de Lesegno C, Verweij F, et al. Mechanical stress and caveolin-1 control the release of extracellular vesicles with increased tumorigenic properties. 2024. doi:10.1101/2024.09.05.611225

112. Ye ZW, Yu ZL, Chen G, Jia J. Extracellular vesicles in tumor angiogenesis and resistance to anti-angiogenic therapy. Cancer Sci. 2023 Jul;114(7):2739–49. doi:10.1111/cas.15801 PubMed PMID: 37010195.

113. Bai Y, Wang X, Shen L, Jiang K, Ding X, Cappetta D, et al. Mechanical Stress Regulates Endothelial Progenitor Cell Angiogenesis Through VEGF Receptor Endocytosis. Int Heart J. 2016 May 25;57(3):356–62. doi:10.1536/ihj.15-387 PubMed PMID: 27150003.

114. Shiu YT, Weiss JA, Hoying JB, Iwamoto MN, Joung IS, Quam CT. The role of mechanical stresses in angiogenesis. Crit Rev Biomed Eng. 2005;33(5):431–510. doi:10.1615/critrevbiomedeng.v33.i5.10 PubMed PMID: 16000089.

115. Goel S, Duda DG, Xu L, Munn LL, Boucher Y, Fukumura D, et al. Normalization of the vasculature for treatment of cancer and other diseases. Physiol Rev. 2011 Jul;91(3):1071–121. doi:10.1152/physrev.00038.2010 PubMed PMID: 21742796.

116. Qiu Y, Lv Z, Du T, Ji P, Zhu X, Yang X, et al. YAP-mediated activation of VEGFA–VEGFR2 signaling in mechanically stimulated fibroblast exosomes enhances angiogenesis. Vol. 50. 2026;50:114442.